

Effect of Atmospheres on the Microstructure Evolution of Sintered Ag Die Attach Layer

Experiments, characterizations, and
Simulations

by

Qilin Xing

<u>Student Name</u>	<u>Student Number</u>
Qilin Xing	5743737

Contents

1	Introduction	1
1.1	Research Background	1
1.1.1	Development Trend of Wide Bandgap(WBG) Semiconductor Devices	1
1.1.2	Die Attach Layer	3
1.1.3	The Role of Ag Sintering Packaging Technology	6
1.2	Research Questions and Objectives	8
1.2.1	Importance of Sintering Process & Aging Process under Different Atmospheric Conditions	8
1.2.2	Objectives and Deliver	9
1.3	Organisation of the Thesis Structure	9
2	Literature Review	10
2.1	Current Status of Research on Silver Sintered Materials	10
2.2	Different Microstructure Characterisation Methods	11
2.2.1	Scanning Electron Microscopy	11
2.2.2	Transmission Electron Microscopy	11
2.2.3	Electron Backscatter Diffraction	12
2.2.4	X-ray Computed Tomography	13
2.3	Morphological Changes and Microstructure Evolution	14
2.3.1	Morphology and Microstructure of the Particles	14
2.3.2	Grain Growth and Abnormal Grain Growth	15
2.3.3	Agglomeration and Coalescence	16
2.4	Modelling and Simulation Methods	17
2.4.1	Molecular Dynamics Simulation	17
2.4.2	Kinetic Monte Carlo Simulation	18
2.4.3	Phase Field Simulation	18
2.5	Shortcomings and Challenges of Current Research	19
2.6	Choice of Methods and Their Advantages	20
3	Experimental Procedures and Microstructure characterisation	21
3.1	Experiment Design and Fabrication Process	21
3.1.1	Design of Experiment	21
3.1.2	Sample Preparation	22
3.1.3	Low-Temperature sintering & Aging Experiment	23
3.2	Sheer Test	27
3.2.1	Experimental Preparation	27
3.2.2	Analysis of Maximum Load Force Variation Under Different Aging and Sintering Conditions	28
3.2.3	Fracture Position Check after Sheer Test by SEM	30

3.3	Microstructure Evolution Analysis During Aging Tests	33
3.3.1	Cross-sectional Images by FIB	33
3.3.2	Comprehensive Microstructural Analysis Using EBSD	35
4	Modelling and Simulation	45
4.1	Modelling of Microstructural Evolution	45
4.1.1	Kinetic Monte Carlo simulation & Potts model	45
4.1.2	KMC-based hybrid Q-state potts & phase field model (QPPF)	46
4.2	Simulation Results and Analysis	47
4.3	Limitations of the Model	51
5	Conclusion	52
A	Pseudocode	59

List of Figures

1.1	Wide bandgap semiconductor technology development timeline	2
1.2	Comparison of power application ranges of SiC and GaN[22]	3
1.3	Chip packaging structure diagram[1]	4
1.4	Schematic diagram of the importance of the chip bonding layer	5
1.5	Global die attach materials market analysis chart[2]	6
1.6	Application of Ag sintering material in semiconductor packaging[3]	7
2.1	Surface morphologies of silver structures a) rough surface b) homogeneous morphology c) nanoflower [11]	11
2.2	Transmission electron microscope image of silver nanoparticles [9]	12
2.3	EBSD-IPF maps of die-attached test pieces prepared with the sintered Ag paste before and after high-temperature exposure at 250 °C: a initial, 0 h; b 250 h; c 500 h; d 1000 h[8]	13
2.4	Nanostructure evolution of silver with T°/time (colors are added to help visualizing only) a) growth of the largest pore (in white) b) projection the pore nanostructure within a thin slab against temperature/time and c) details of pore evolution in 3D. White dotted arrows show pore disappearance. Solid blue arrows shows pore growth[27]	14
2.5	SEM images of the nanoscale silver paste (a) before and (b) after sintering on silicon substrate at 280 °C [8]	15
2.6	The microstructures of the silver annealed at 600 °C in vacuum for (a) 10 min, (b) 20 min, (c) 2 h, and (d) 10 h [47]	16
2.7	The schematic diagram of abnormal grain growth for nt-Cu films annealed at different temperatures: (a) below critical abnormal grain growth and (b) above critical abnormal grain growth [47]	17
2.8	Geometric parameters for the tensile molecular dynamic simulation [52]	17
2.9	Sintered silver powder particles in a (a) before grain growth, (b) after grain growth, color indicates grain orientation [52]	18
2.10	Evolution of two equal-sized silver particles under isothermal sintering of 400 °C for different times [52]	19
3.1	Influence of the input factors (i.e., design, process and Ag paste formulation) on the microstructural properties (i.e., porosity, grain sizes, and interfacial properties) and the resulting mechanical, electrical and thermal properties of the sintered Ag joint[45]	21
3.2	schematic of the device structure	22
3.3	Schematic diagram of sintering silver paste position	23
3.4	Top view of sample	23
3.5	Flowchart of sintering and aging processes	23

3.6	Schematic diagram of sintering and aging treatment processes under different atmospheres	24
3.7	Temperature variation over time during sintering	25
3.8	Mounting diagram	26
3.9	Schematic diagram of cross-sectional sample	26
3.10	Shear direction test diagram	27
3.11	Relationship between aging time and maximum load force aging in an air environment	28
3.12	Relationship between aging time and shear strength in a nitrogen environment	29
3.13	Variation of shear strength with aging time under different sintering conditions	30
3.14	Thermal aging microstructure evolution of pure silver aging at 200°C in air environment	31
3.15	Thermal aging microstructure evolution of pure silver aging at 200°C in nitrogen environment	32
3.16	Thermal aging microstructure evolution of pure silver aging at 200°C in air environment with different sintering condition	33
3.17	Comparison of microstructures of pure silver sintered materials at 200°C in air and nitrogen environments after thermal aging in nitrogen	34
3.18	Comparison of microstructures of pure silver sintered materials at 200°C in air and nitrogen environments after thermal aging in air	35
3.19	Thinned sample wrapped with copper tape	36
3.20	Inverse Pole Figure of thermal aging of pure silver sintered material at 200°C in air environment	37
3.21	Surface energy variation with different defect mechanisms[13]	38
3.22	Inverse Pole Figure of thermal aging of pure silver sintered material at 200°C in Nitrogen environment	38
3.23	Relationship between grain size and area fraction after thermal aging at 200°C in air	39
3.24	Relationship between grain size and area fraction after thermal aging at 200°C in nitrogen	40
3.25	Comparison of grain size with IPF+TOP figure	41
3.26	Grain growth fitting curves of L1 and L3 groups	42
3.27	Kernel Average Misorientation figure of thermal aging of pure silver sintered material at 200°C in air environment	43
3.28	Kernel Average Misorientation figure of thermal aging of pure silver sintered material at 200°C in nitrogen environment	43
4.1	Simulation of the microstructure evolution of pure silver sintered material during sintering in air (starting from 0 hours)	47
4.2	Microstructure evolution of pure silver sintered material during sintering in air (0h, 168h, 504h, 1008h)	48
4.3	Energy change over time during system stabilization	49
4.4	Phase evolution during aging process under air environment	50
4.5	Volumetric free energy variation with composition for different phases	51

List of Tables

1.1	Comparison of wide bndgap semiconductors vs traditional semiconductors . .	2
3.1	Experimental sintering and aging conditions diagram	25
3.2	Key parameters from the shear test	27

1

Introduction

1.1. Research Background

1.1.1. Development Trend of Wide Bandgap(WBG) Semiconductor Devices

Wide bandgap semiconductors, also known as third-generation semiconductors, are materials with a larger bandgap energy than traditional semiconductors such as silicon. The bandgap of WBG materials is typically more than 2 eV[37, 28], which gives them excellent electrical and thermal properties. Major WBG materials include SiC and GaN. These materials enable devices to operate at higher voltages and temperatures, making them a necessity for advanced power electronics and optoelectronics.[42, 41]

Historical Evolution and Milestones

The development of WBG semiconductor devices has gone through several key stages, driven by the demand for higher performance electronic products. Initially, from the 1950s to the 1980s, research focused on the basic properties of materials such as SiC and GaN; from the 1990s to the 21st century, major advances in material growth technology, such as physical vapor transport for SiC and metal organic chemical vapor deposition for GaN, promoted the commercialization of SiC devices and GaN-based LEDs. Since the beginning of the 21st century, improvements in performance and reliability have led to the widespread use of WBG devices in automotive, renewable energy and telecommunications applications, while GaN-on-Si technology has continued to innovate and expand its use in power conversion and RF systems.[43, 8]

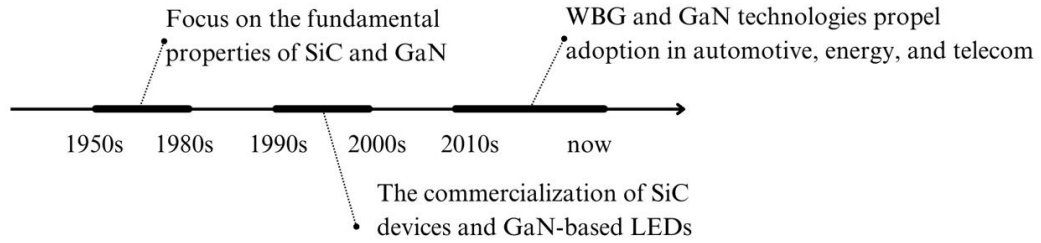


Figure 1.1: Wide bandgap semiconductor technology development timeline

Pros and Cons

Compared with traditional semiconductors, WBG semiconductors have multiple intrinsic advantages, such as higher breakdown voltage, excellent thermal conductivity and lower on-resistance, which have promoted their widespread use in high-voltage, high-power applications. Key technological advances such as CVD and MOCVD and the development of device structures such as MOSFET and HEMT. In addition, the reliability and performance of WBG devices have been significantly improved by reducing material defects and innovative thermal management schemes. [5, 14, 36]

Feature	Wide Bandgap Semiconductors (WBG)	Traditional Semiconductors
Bandgap Energy	Higher (SiC: 3.26 eV, GaN: 3.4 eV)	Lower (Si: 1.12 eV)
Thermal Conductivity	Better (SiC: 490 W/mK)	Lower (Si: 150 W/mK)
Operating Temperature	Higher (up to 600°C)	Lower (up to 150°C)
Efficiency	Higher energy efficiency	Lower energy efficiency
Size and Weight	Smaller and lighter	Larger and heavier
Maturity of Technology	Less mature, newer technology	More mature, well-established
Application Areas	High-power, high-frequency	Broad range, including consumer electronics

Table 1.1: Comparison of wide bandgap semiconductors vs traditional semiconductors

Application and Challenges

WBG semiconductor devices are penetrating various markets due to their superior performance characteristics. These devices play a vital role in multiple fields. In the automotive industry, SiC MOSFETs and GaN transistors are used in power inverters, on-board chargers[35, 24], and DC-DC converters for electric and hybrid vehicles to improve efficiency, reduce weight, and extend battery life. In the renewable energy sector, WBG devices improve the efficiency of solar inverters while improving the reliability of electronic systems in wind turbines. In the industrial sector, WBG devices promote efficient operation of motor drives and reduce energy losses. The telecommunications industry uses WBG semiconductors to improve the efficiency of 5G base stations, while data centers use them to reduce energy consumption and heat generation. In the aerospace and defense sector, GaN devices excel in high-power RF applications and electric aircraft, providing high power density and reliability.[15, 30]

However, despite their many advantages, WBG semiconductors still face several challenges. These challenges include high defect density, high cost, thermal management, and

integration with existing systems[21]. Advances in epitaxial growth technology and substrate engineering are needed to improve material quality. Costs can be reduced by optimizing processes and scaling up production. Efficient thermal management solutions include innovative high thermal conductivity substrate materials and improved packaging techniques[44].

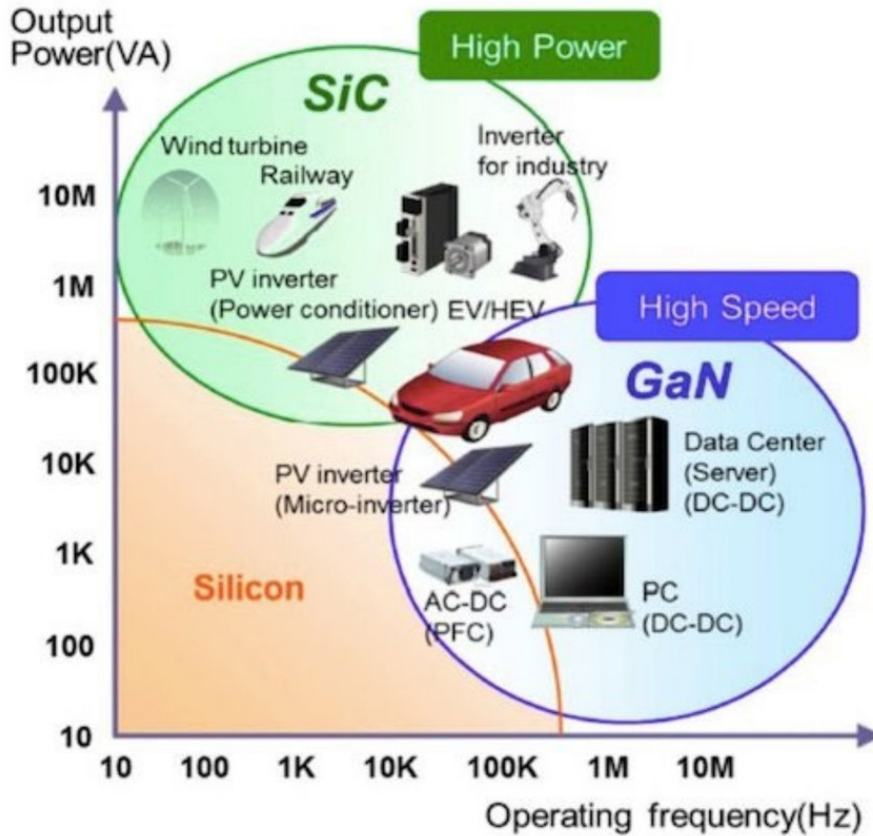


Figure 1.2: Comparison of power application ranges of SiC and GaN[22]

The future of WBG semiconductors is promising, with research focusing on exploring new materials and new packaging technologies to advance device miniaturization and high-density integration for applications such as portable devices and aerospace. Improving device reliability and service life, optimizing energy efficiency, and promoting sustainable energy solutions are also key directions. In addition, emerging applications of WBG devices in electric aviation, quantum computing, and advanced electronic systems demonstrate their broad potential and application prospects[17].

1.1.2. Die Attach Layer

The die bonding layer is the layer that fixes the chip to the substrate during the semiconductor packaging process, and has a crucial impact on the reliability, thermal performance, and electrical performance of the entire semiconductor device. The main functions of the die bonding layer include fixing the chip, maintaining the thermal and electrical connection between the substrate and the chip, and releasing internal stress. Common die bonding materials include silver paste, epoxy resin, eutectic solder, and conductive adhesive. The selection of these materials needs to consider the application requirements of the package, the use environment, the

cost, and the matching performance of other packaging materials[1].

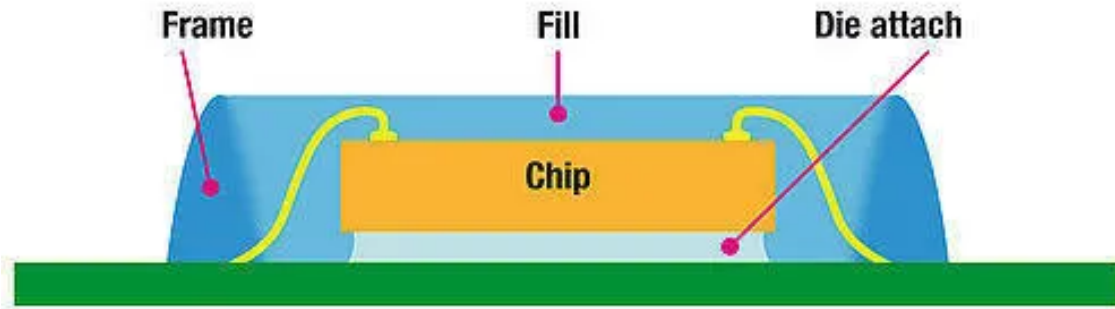


Figure 1.3: Chip packaging structure diagram[1]

Importance of the Die Attach Layer

The die attach layer is an important composition of semiconductor packaging and is the key bonding layer on the package. This layer is critical to the overall performance, reliability and life of the semiconductor device, and is therefore very important in the packaging process[5, 14, 36].

First, the role of the die attach layer is to fix the chip to the substrate. Any movement of the chip will cause it to separate from the substrate, resulting in device failure. Second, the die attach layer plays a key role in thermal management. Since semiconductor devices generate heat during operation, effective heat dissipation is required to prevent overheating. [35, 24].

In addition to mechanical and thermal functions, the die attach layer also has an electrical function. The die attach layer provides a conductive path between the chip and the substrate, ensuring that the resistance is minimized. [15, 30] Another important function is stress relief. Semiconductor devices and their substrates usually have different thermal expansion coefficients, which causes internal stresses during repeated use of the device due to constant temperature changes. These stresses can cause cracking or delamination, resulting in device failure. The die attach layer can absorb and release these stresses, thereby improving the reliability and life of the device[25].

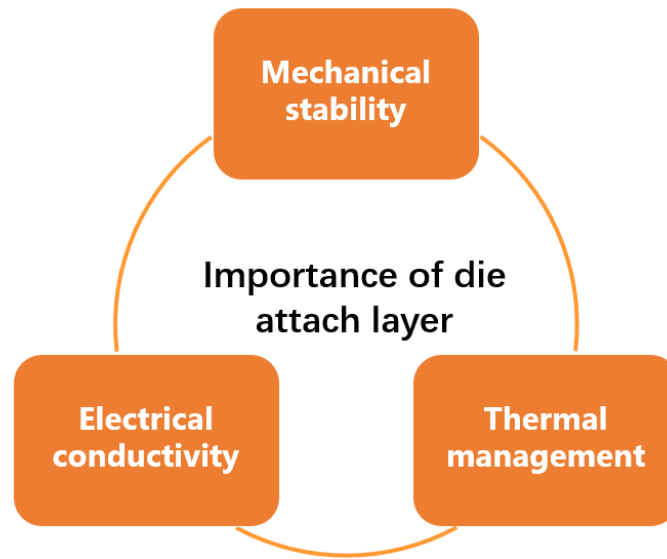


Figure 1.4: Schematic diagram of the importance of the chip bonding layer

In summary, the die attach layer is critical to ensuring the mechanical stability, effective thermal management and electrical performance of semiconductor devices.

Challenges in Die Attach and Advances in Die Attach Technology

Chip packaging technology faces challenges due to the increasing complexity of modern electronics. One of the main issues is thermal management, as the die attach material must effectively dissipate heat, especially in high-power applications[44]. Another major issue is that the temperature of the device will continue to change during operation, which can cause cracks. Compatibility between the die attach material and the chip and substrate is also important, as mismatched thermal expansion coefficients can cause connection failures. In addition, good mechanical properties are also important. It is difficult to maintain good mechanical properties in a material that maintains good thermal conductivity. Other challenges include maintaining high electrical conductivity and low cost[6].

To meet these challenges, advances in die attach technology have introduced various innovative solutions. Among them, silver sintering is an advanced high-temperature solution that has excellent thermal and electrical conductivity while being lead-free and environmentally friendly[43, 42]. Epoxy-based conductive adhesives are also constantly improving to provide better thermal performance. Nanotechnology has brought nano-enhanced materials, which are essential for micro devices. Copper interconnect devices technology is being developed, which has good electrical and thermal conductivity, but oxidation is a serious problem. Hybrid bonding techniques combine materials such as epoxy and metal sintering to achieve a balance between mechanical strength and thermal management[43, 41]. Finally, advances in automation and precision placement technologies have improved the accuracy of the die attach process, reducing errors and increasing yields, and these innovations are helping to address key challenges in die attach technology.

The global die attach materials market, valued at USD 1.45 billion in 2022, is expected

to grow at a CAGR of 5.3%[2], driven by rising demand from the semiconductor industry. The Asia-Pacific region accounted for 34.8% of global market revenue, reflecting its strong presence in electronics manufacturing. The die bonder segment is forecasted to register a CAGR of 5.4%[2], indicating rapid growth in precision bonding technologies. The market is fairly consolidated, with a few key players dominating, and growth is primarily fueled by advancements and increasing demand in semiconductor applications[2].

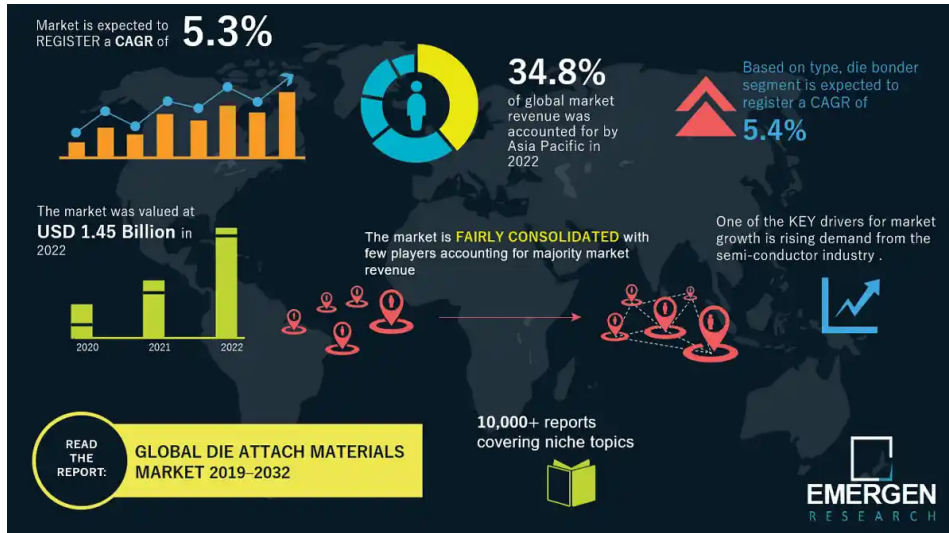


Figure 1.5: Global die attach materials market analysis chart[2]

1.1.3. The Role of Ag Sintering Packaging Technology

Why We Choose Ag Sintering Material

There are many materials that can be used for die-attach, such as silver, copper and other alloys. However, due to the need to work at high temperatures, SiC power modules not only need to have the above-mentioned heat resistance, but also must have good reliability and conductivity.

In terms of conductivity, the lower the resistance of the chip attachment material, the smaller the power loss. Silver is an excellent conductive material, which can reduce the power loss in the device. At the same time, traditional Sn-based solders are more likely to fail in high-temperature environments, and high-melting-point materials such as silver have excellent thermal stability, but heat resistance and conductivity are not the only considerations.[38]

When the power module is working, the temperature rise rate of different parts between the chip and the substrate is different, the thermal expansion coefficient is different, and the expansion degree is also different, so strain and stress will be generated inside. At present, although silver itself has good thermal conductivity, the strength and ductility of sintered silver are poor, which can easily cause cracks or fractures in the sintered silver material itself, which is also the main problem of sintered silver material as a die-attach material.[4]

In summary, the ideal SiC power module chip attachment material should have heat resistance, good mechanical properties and conductivity, and be able to work stably for a long time under high temperature and complex stress conditions. In order to meet these requirements, sintered silver, full copper, and some alloy materials have become the focus of research. The development and application of these materials can not only improve the working efficiency of SiC power modules, but also extend their service life.

Application of Ag sintering Material in Semiconductor Packaging

Silver sintering materials are widely used in semiconductor packaging, especially in electronic devices that require high performance and high temperature requirements. IGBT, MOSFET and other power electronic devices [49] usually use sintered silver materials because silver materials have excellent electrical conductivity at high temperatures. In addition, in addition to high-power applications, silver sintering materials can also remain stable under ultra-high temperature conditions of 250°C[51], so they are suitable for fields that require high-temperature operation, such as automobiles and aerospace. At the same time, LEDs [18] and optoelectronic compositions[53] use the high heat dissipation of silver powder materials to make the equipment have long-lasting availability and support the miniaturization and high power density design of the equipment. In one of the advanced technologies of three-dimensional packaging[56], silver sintering materials are not only effective adhesives, but also can solve the heat dissipation problems caused by packaged memory. Because sintered silver materials are very prominent in various application fields[3], they have become key materials for power devices, wide bandgap semiconductors, and various packages, and have a place in various companies such as automobiles, aerospace, 5G communications, and renewable energy.

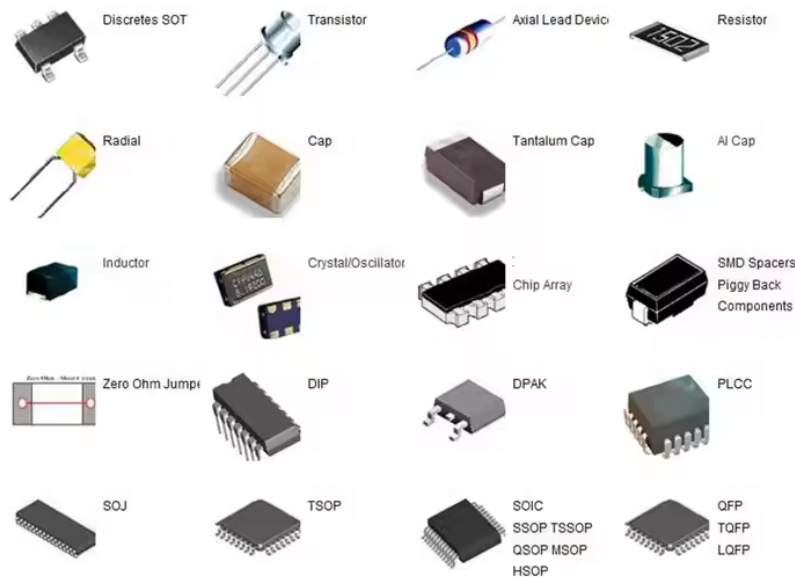


Figure 1.6: Application of Ag sintering material in semiconductor packaging[3]

Problems that Sintered Silver Materials still Face

Among these issues, insufficient reliability is considered one of the most common factors leading to power device failure. Structural changes can affect the long-term mechanical stability and performance of sintered silver, especially under severe thermal cycling and high temperature conditions common in power electronics applications.

Thermal migration occurs when silver atoms move from hotter areas to cooler areas under the influence of thermal gradients[7]. This phenomenon is particularly problematic in high-power devices where localized heating occurs. As the silver atoms migrate, holes form in hot areas and material agglomeration occurs in cooler areas, ultimately leading to delamination or failure of the die attach layer[7]. This effect is particularly evident in environments with rapid thermal cycling, as the thermal gradient is constantly changing, causing significant redistribution of the material.

The microstructure of sintered silver changes significantly under the influence of high temperatures, especially when exposed to temperatures exceeding 200°C. Grain growth and enlargement of holes are common phenomena[50]. Grains will become larger and holes will slowly agglomerate over time[4], which will be analyzed in detail in the third chapter. This grain growth will become less obvious as the grain boundaries become less obvious, resulting in a weakened ability of the material to absorb and redistribute internal stress, making it more susceptible to cracking under mechanical shock.

Thermal shock is also one of the important influencing factors. This requires that the chip attachment material can withstand alternating loads of low and high temperatures of 300°C in addition to high temperatures of up to 250°C. Liu et al. [23] prepared a sintered silver joint at 250°C. After 1000 cycles of thermal shock, the microstructure deteriorated significantly, the substrate also cracked, and the strength dropped from 37.6 MPa to about 5.0 MPa, a decrease of 86.7%. Xu et al.[48] used a modified DBC(Direct Bonded Copper) substrate to replace the original sintered silver joint at 250°C for 5 minutes. After 1000 thermal shock cycles in the range of -50°C to 250°C, the strength of the ornament also dropped from 81.9 MPa to 8.2 MPa, with a difference of 64.3 MPa. When thermal shock occurs, the mechanical properties of sintered silver decrease slightly[39].

In order to solve these challenges, how to change the ductility and strength of the material by controlling different sintering and aging conditions such as atmosphere time is a good way.

1.2. Research Questions and Objectives

Sintered silver has excellent thermal conductivity and must also have good electrical conductivity, but it still has many problems. For example, high porosity leads to decreased mechanical strength, and higher porosity reduces shear strength[55]; silver migration is a serious problem, which leads to decreased mechanical strength, especially in high temperature environments[54]; and when combined with a copper substrate, copper oxidation forms an oxide layer, which increases interface resistance and affects connection reliability[40]. In addition, sintered silver requires longer sintering times than traditional solders and has poor compatibility with existing manufacturing processes, which may increase process complexity and cost. So the question I want to explore is how to reduce the reliability issues of silver, namely silver migration, microstructural changes and fractures that occur under different sintering, aging atmospheres and aging times.

1.2.1. Importance of Sintering Process & Aging Process under Different Atmospheric Conditions

In order to explore how to improve the reliability of sintered silver as a chip bonding material while ensuring that it retains excellent electrical and thermal conductivity, it was found that the

atmosphere and aging time have a great influence on the mechanical properties and reliability of sintered silver. In the literature review, it was mentioned that Chuangtong Chen (2018) et al.[8] used air and nitrogen atmospheres during the sintering process, and the temperature was increased from 25 °C to 250 °C which is 10 °C/min , and the mechanical properties of their products were finally improved. Chen (2020) et al.[9] also only used air sintering atmosphere at 250 °C for 30 minutes, and the strength, deformation resistance and hardness of the final product were improved. K.S.Siow et al. (2014) [11]sintered in different atmospheres of air, nitrogen and a mixture of the two, heating from 30 °C to 250 °C, and the shear strength of their products increased. K.S.Siow (2020)[46] sintered micron-sized Ag particles at 230 °C in air and nano-sized Ag particles at 250 °C, and the hardness of the final product increased. Chulumin Oh et al. [33] sintered in a pure nitrogen atmosphere, heating from 25 °C to 225 °C and maintaining for 90 minutes. The final product increased in strength but decreased in weight. Seonhee Jang (2021) et al. [20]heated from 80 °C to 220 °C in an atmosphere of nitrogen-bubbled formic acid for 12 min, and the mechanical properties of the final product were significantly improved.

1.2.2. Objectives and Deliver

- Objectives: Understand the structural changes of sintered silver materials in different sintering atmospheres, aging atmospheres, and aging times, as well as the microscopic mechanism of silver migration and its impact on its reliability.
- Deliver: Describe the changes in microstructure through characterization methods and replicate them using simulation methods.

1.3. Organisation of the Thesis Structure

The thesis is structured into several key chapters. It begins with an Introduction, which outlines the research background, including the development of wide bandgap semiconductors, the importance of die attach materials, and the role of Ag sintering technology in semiconductor packaging. This is followed by a Literature Review, which surveys existing studies on silver sintering materials and various microstructure characterization methods. Next, the Experimental Procedures and Microstructure Characterization chapter details the design, fabrication, and testing processes used, including methods like FIB and EBSD. The Modeling and Simulation chapter explores the computational methods used to analyze microstructural evolution, such as Monte Carlo simulations and phase field models. Finally, the Conclusion summarizes the findings.

2

Literature Review

My literature review was completed on June 16, and the following is a summary of it.

2.1. Current Status of Research on Silver Sintered Materials

As a high-temperature electronic packaging material that has attracted much attention, silver sintering technology has been widely studied and applied in recent years, especially in the field of wide bandgap semiconductor power devices [29]. Wide bandgap semiconductor materials can work in harsh environments of high voltage, high temperature and high frequency, requiring packaging materials to have extremely high thermal conductivity, electrical conductivity and high temperature resistance [10]. Traditional solders cannot maintain performance stability under these extreme conditions due to their low melting point, and therefore cannot meet the needs of these emerging applications [42].

In contrast, silver sintered materials represent a promising solution due to their excellent electrical and thermal conductivity [8]. The melting point of silver is 961 °C, and silver nanoparticles can be sintered at lower temperatures of 150-300 °C, maintaining their excellent electrical and thermal conductivity properties, making them suitable for high-power, high-temperature applications [46]. Silver sintering technology is not only used in the packaging of high-power semiconductor devices, but is also widely used in 5G communications, consumer electronics, aerospace and other fields [33, 20]. Although silver sintered materials show good application prospects, they still face many challenges in practical applications. One of the most significant problems is the coarsening of the microstructure. Silver particles are prone to agglomeration during the sintering process, leading to the formation of pores, thereby reducing the mechanical properties and electrical conductivity of the material [11]. Pore diffusion is also an important factor affecting the reliability of the silver sintered layer. The existence of pores will not only reduce the strength of the material, but also trigger the generation of cracks. In addition, at high temperatures, silver electromigration and silver migration phenomena can lead to the formation of silver whiskers, increasing the risk of short circuits [39].

In response to these problems, researchers have tried various methods to optimize the microstructure of silver sintered materials. For example, Chuangtong Chen et al. (2018) successfully improved the mechanical properties of silver sintered materials by gradually raising the

temperature in air and nitrogen environments [8]. Pure air atmosphere sintering can also significantly improve the strength and deformation resistance of the material. Research also shows that different sintering atmospheres have a significant impact on material properties, and a mixed atmosphere of nitrogen and air can significantly improve shear strength [42]. Future research will further focus on the optimization of the silver sintering process and explore how to reduce pores and improve electrical and thermal conductivity by adjusting particle size, sintering atmosphere, temperature, and other conditions, thereby improving the overall performance and long-term reliability of the material [20, 52].

2.2. Different Microstructure Characterisation Methods

Characterization of microstructure is the key to understanding the performance and reliability of silver sintered materials. The microstructure directly affects the mechanical strength, electrical conductivity, thermal conductivity and other properties of the material, so it is crucial to accurately characterize the microstructure of silver sintered materials [41]. The following are several common characterization methods and their applications.

2.2.1. Scanning Electron Microscopy

Scanning electron microscopy is one of the most commonly used characterization tools in materials science research, mainly used to observe the surface morphology of materials [11]. SEM generates high-resolution images through the interaction of electron beams with samples to analyze the surface characteristics of silver sintered materials. This method can effectively reveal the distribution of silver particles, morphological changes before and after sintering, and pore structure. During the sintering process, silver particles fuse and leading the formation of pores. SEM can clearly show this change, especially the reduction of porosity after sintering and the density of inter-particle bonding.

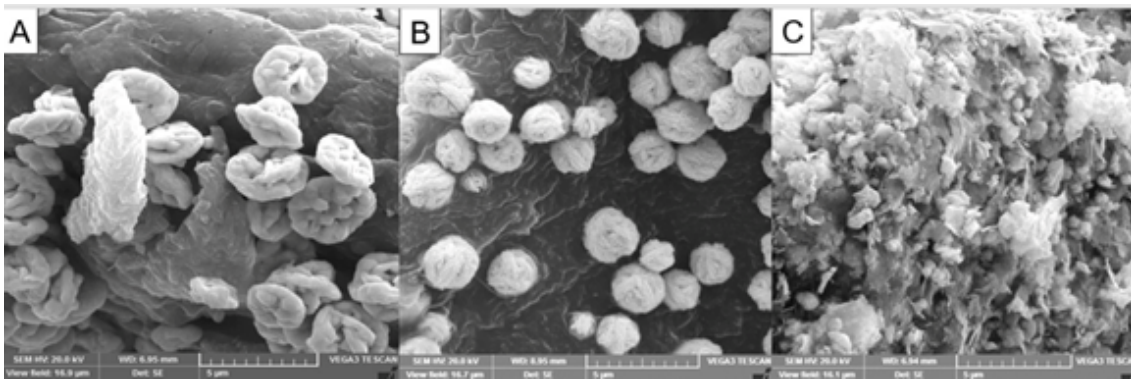


Figure 2.1: Surface morphologies of silver structures a) rough surface b) homogeneous morphology c) nanoflower [11]

2.2.2. Transmission Electron Microscopy

Transmission electron microscopy is a powerful tool for observing the internal structure of materials, especially for nanoscale research. By transmitting an electron beam through the sample, TEM can generate extremely high-resolution images for analyzing the crystal structure, grain boundaries, defects and other information of nanosilver particles [11].

In the study of silver sintered materials, TEM can show the merging of particles and the growth of grains during the sintering process, which is crucial for understanding the interaction between particles and their impact on the overall performance [9].

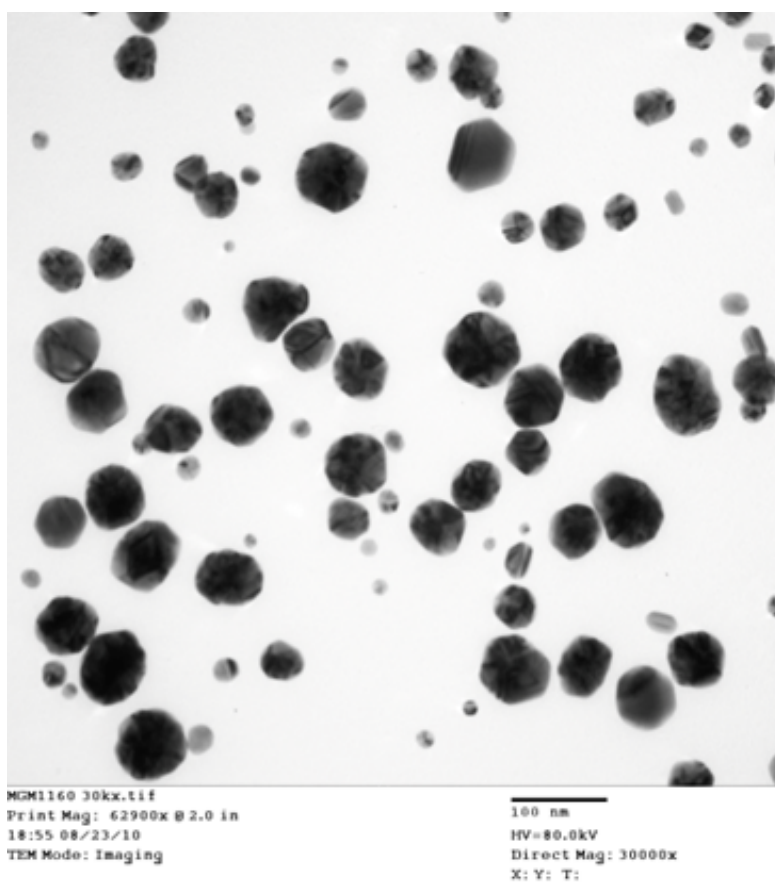


Figure 2.2: Transmission electron microscope image of silver nanoparticles [9]

As shown in **Figure 2.2**, the TEM image shows silver nanoparticles of different sizes and morphologies. The particle size distribution is relatively uniform, and the morphology is mainly spherical.[33, 20].

2.2.3. Electron Backscatter Diffraction

Electron backscatter diffraction is a technique commonly used for crystal structure analysis, usually combined with SEM. EBSD can provide detailed information about the material's grain orientation, grain boundaries, and crystal defects. This is important for studying the rearrangement and growth of grains during silver sintering, especially during high-temperature aging, where EBSD can reveal the evolution of grains [8].

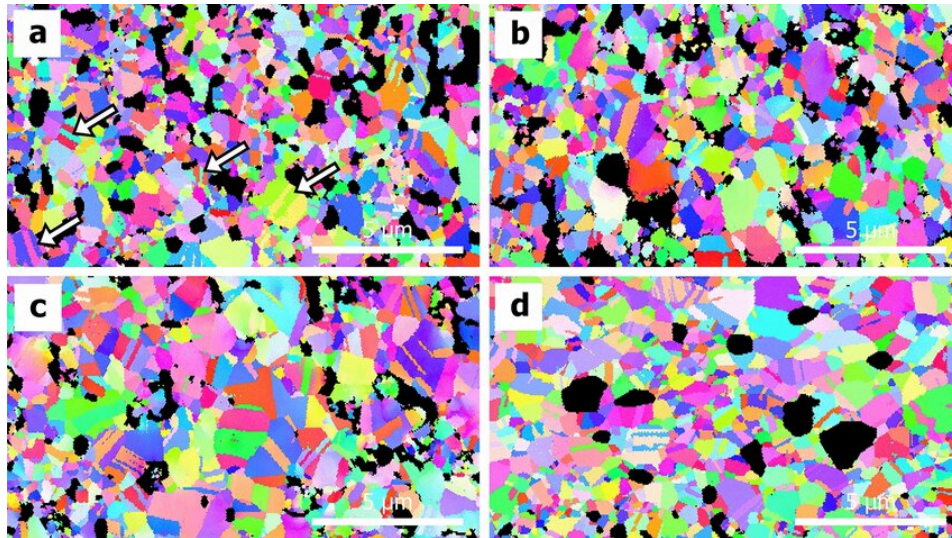


Figure 2.3: EBSD-IPF maps of die-attached test pieces prepared with the sintered Ag paste before and after high-temperature exposure at 250 °C: a initial, 0 h; b 250 h; c 500 h; d 1000 h[8]

It can be seen from **Figure 2.3** that the silver particles undergo significant grain growth under high-temperature exposure, especially after long-term exposure, the grains become bigger and more uniform.

2.2.4. X-ray Computed Tomography

X-ray computed tomography is a non-destructive testing technique that can observe the internal structure of samples in three dimensions. It is particularly suitable for studying the porosity and particle distribution of silver sintered materials. By using in-situ X-rays to see through the samples and generate 3D images, researchers can observe the microstructural changes of materials at different temperatures[27].

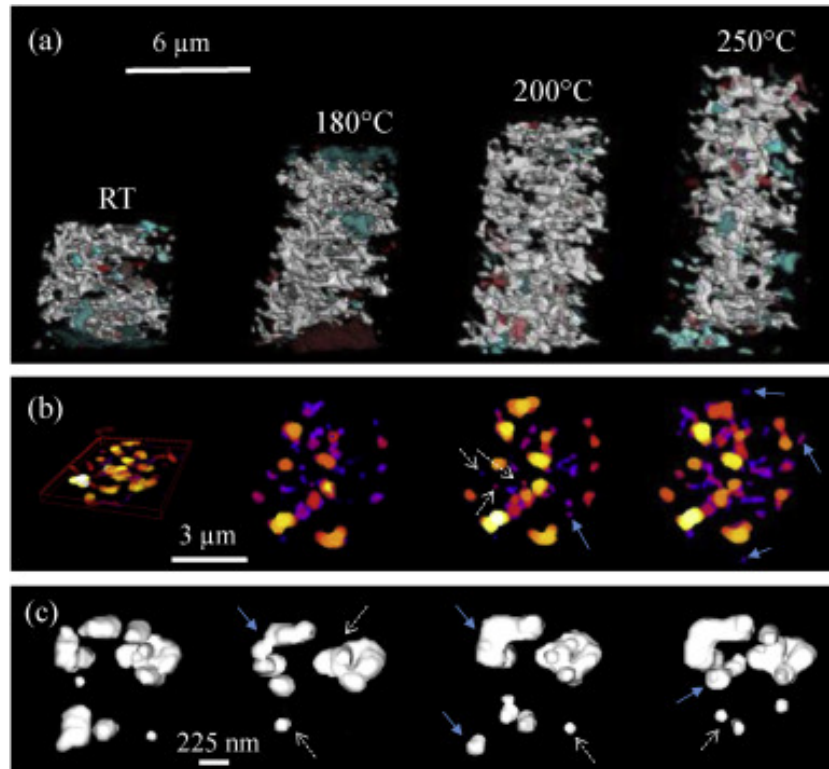


Figure 2.4: Nanostructure evolution of silver with T° /time (colors are added to help visualizing only) a) growth of the largest pore (in white) b) projection the pore nanostructure within a thin slab against temperature/time and c) details of pore evolution in 3D. White dotted arrows show pore disappearance. Solid blue arrows shows pore growth[27]

As shown in the **Figure 2.4**, XCT images show the evolution of the pore structure of silver sintered materials at different temperatures. As the temperature increases, the pores in the material gradually decrease and the structure becomes denser.

2.3. Morphological Changes and Microstructure Evolution

2.3.1. Morphology and Microstructure of the Particles

During the sintering process of silver sintered materials, the morphology and microstructure of the particles undergo significant evolution. Initially, the particles are well-dispersed with clear boundaries. As the sintering progresses, the particles begin to fuse, and the microstructural changes lead to enhanced mechanical, electrical, and thermal properties [34]. These changes are crucial for applications where reliable electrical connectivity and high thermal conductivity are required.

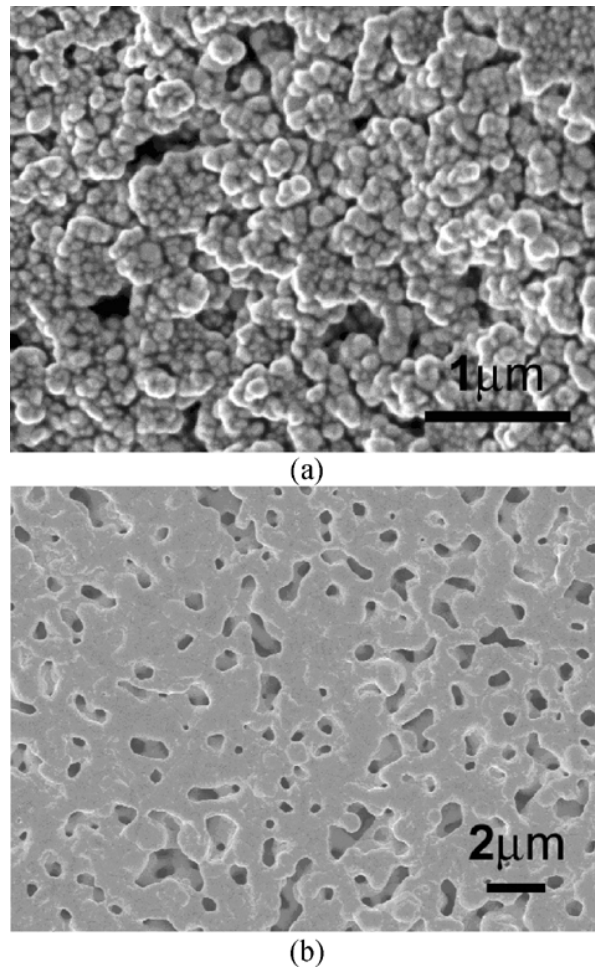


Figure 2.5: SEM images of the nanoscale silver paste (a) before and (b) after sintering on silicon substrate at 280 °C [8]

As shown in the **Figure 2.5**, before sintering, the silver particles are dispersed with clear boundaries and large pores; after sintering, the particles gradually fuse, the pores are significantly reduced, and the connections between particles are enhanced. This densification improves the material's electrical conductivity, as the reduction in porosity minimizes resistive pathways. Additionally, the enhanced inter-particle connections lead to better mechanical strength, reducing the risk of failure during use [31].

2.3.2. Grain Growth and Abnormal Grain Growth

Grain growth is another important microstructural evolution phenomenon during the sintering process. Under high-temperature conditions, silver particles gradually form larger grains through diffusion and rearrangement, and the interface between grains is reduced, thereby improving the thermal and electrical conductivity of the material [42]. However, Abnormal Grain Growth (AGG) sometimes occurs under different conditions, causing a few grains to be significantly larger than the surrounding grains, forming an uneven microstructure. This uneven grain structure can negatively impact the material's mechanical properties, such as reducing its strength and toughness [33].

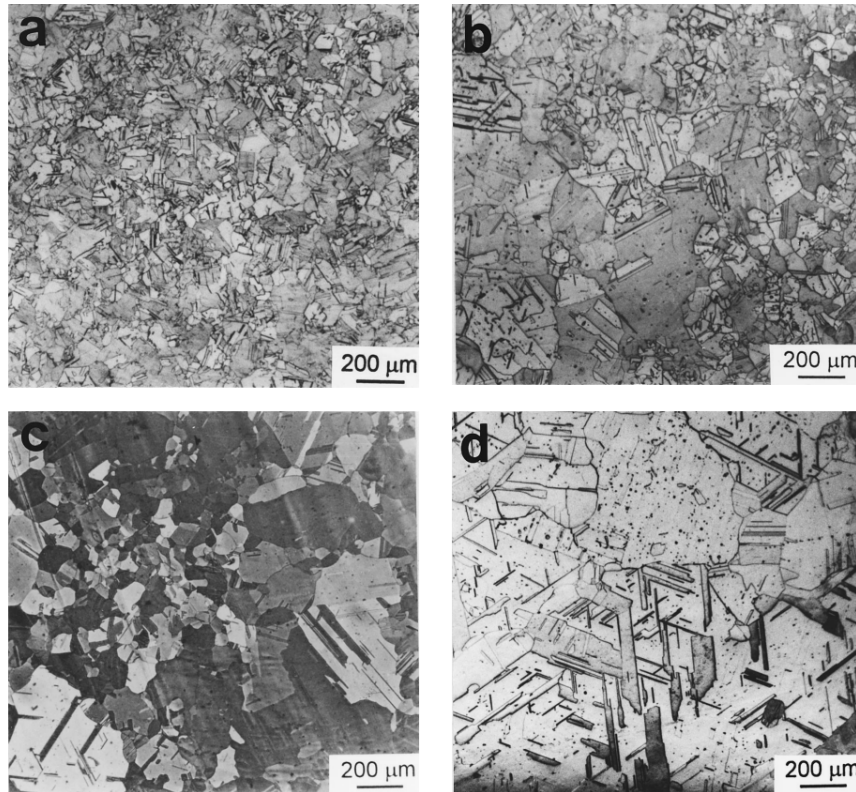


Figure 2.6—The microstructures of the specimens annealed at 600 °C in vacuum for (a) 10 min, (b) 20 min, (c) 2 h, and (d) 10 h.

Figure 2.6: The microstructures of the silver annealed at 600 °C in vacuum for (a) 10 min, (b) 20 min, (c) 2 h, and (d) 10 h [47]

Figure 2.6 above shows the grain growth process of silver particles at a high temperature of 600 °C. In the early stage of sintering, the particles are still small and closely arranged; as the sintering time increases, the grains gradually increase and form a polygonal structure. After 2 hours and 10 hours of annealing, the grain size increases further and the grain boundaries become more obvious. This grain growth process is a typical feature of the microstructural evolution of silver sintered materials [10, 20].

2.3.3. Agglomeration and Coalescence

Silver nanoparticles are prone to agglomeration and coalescence during sintering due to their large surface area. At lower temperatures, silver particles contact each other through surface diffusion mechanisms and form necks [34, 9]. As the temperature rises, the particles further fuse to form a dense structure. However, the agglomeration phenomenon can cause the density of particles in local areas to be too high, resulting in an uneven overall structure, which affects the mechanical and electrical properties of the material.

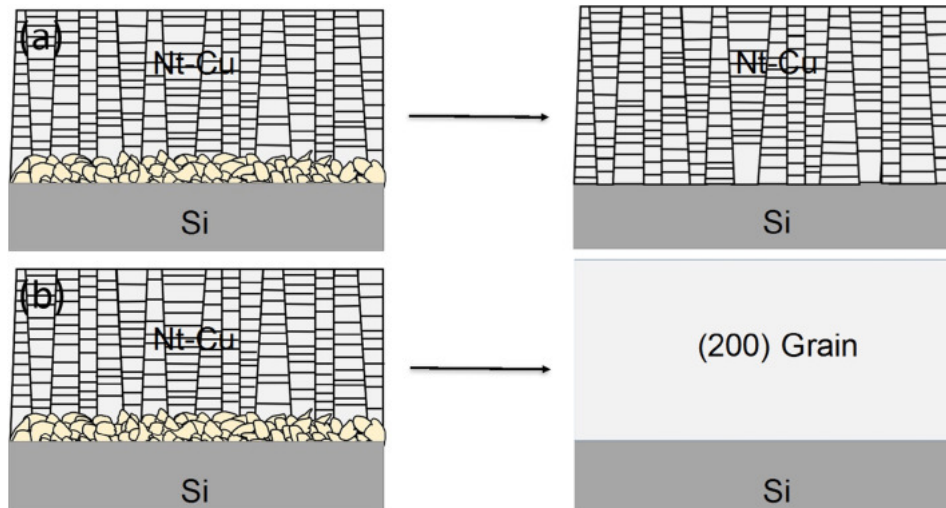


Figure 2.7: The schematic diagram of abnormal grain growth for nt-Cu films annealed at different temperatures: (a) below critical abnormal grain growth and (b) above critical abnormal grain growth [47]

As shown in the **Figure 2.7**, abnormal grain growth can cause some grains to grow significantly during the annealing process, forming a large-area grain structure. This situation often reduces the overall uniformity and reliability of the material [33, 20].

2.4. Modelling and Simulation Methods

Simulation and modeling methods play an important role in understanding the microstructural evolution of silver sintered materials. Through different modeling methods, researchers can predict the behavior of materials under different conditions from atomic to macroscopic scales, helping to optimize the sintering process [52, 29].

2.4.1. Molecular Dynamics Simulation

Molecular dynamics simulation is an atomic-scale simulation method that reveals the diffusion and rotation behavior of particles by tracking the motion of atoms and molecules. MD simulation can describe in detail the interaction between silver nanoparticles during the sintering process and the energy exchange between particles [17].

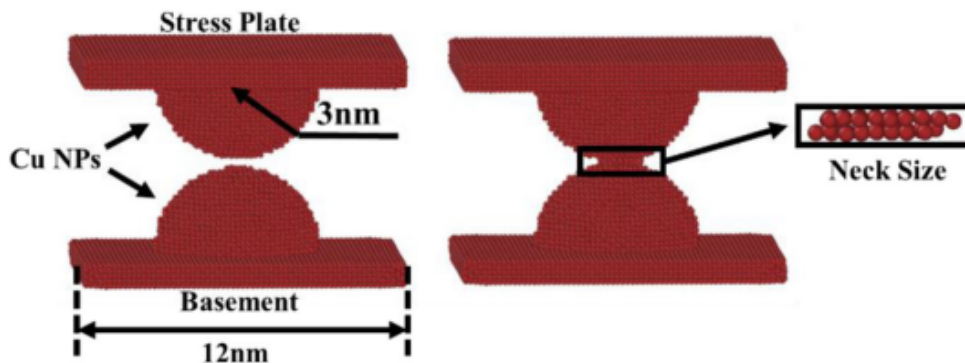


Figure 2.8: Geometric parameters for the tensile molecular dynamic simulation [52]

MD simulations can not only predict the microstructural changes of particles during sintering, but also describe the changes in the resistivity of the material over time.

2.4.2. Kinetic Monte Carlo Simulation

Kinetic Monte Carlo simulation is a method that simulates the energy minimization process of a system by random sampling. It is particularly suitable for simulating the grain growth and pore migration of silver sintering materials during the sintering process [52].

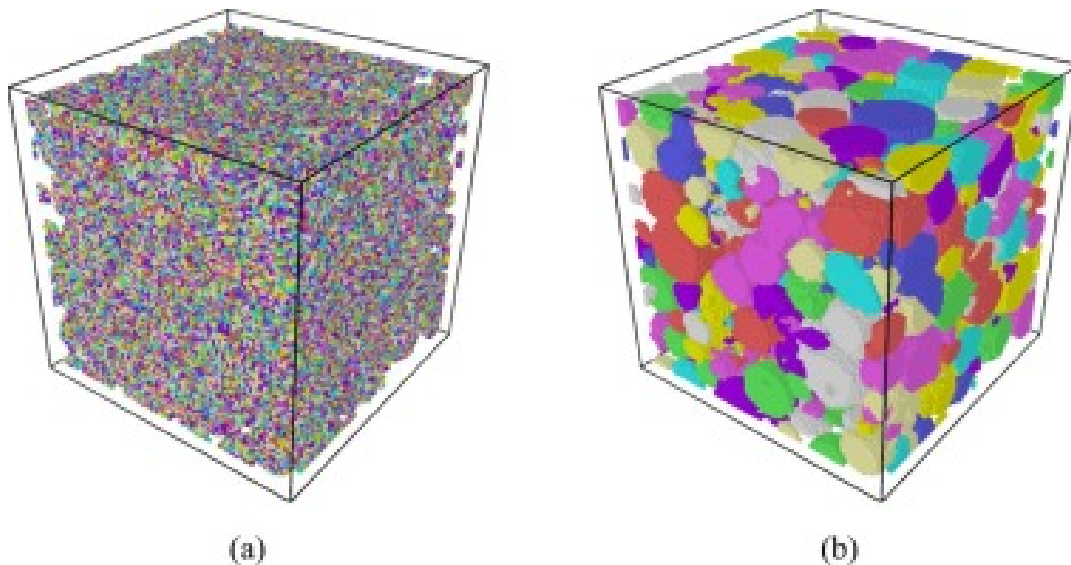


Figure 2.9: Sintered silver powder particles in a (a) before grain growth, (b) after grain growth, color indicates grain orientation [52]

KMC simulations are able to predict the microstructural evolution of silver particles, and by observing the changes in the particles before and after sintering, their impact on material properties can be analyzed .

2.4.3. Phase Field Simulation

The phase field method is a continuous field method used to describe material phase changes and grain growth. Unlike the KMC method, the PF method describes the microstructure of the material by introducing continuous phase field variables and simulates the evolution of the microstructure by minimizing the free energy functional. The advantage of the PF method is that it can naturally and continuously describe the evolution of complex microstructures such as grain interfaces and phase interfaces. The field method itself does not directly simulate the chemical composition of nitrogen, oxygen or reducing gases, but reflects different sintering atmospheres by adjusting physical parameters in the model such as diffusion coefficients and chemical potentials[32].

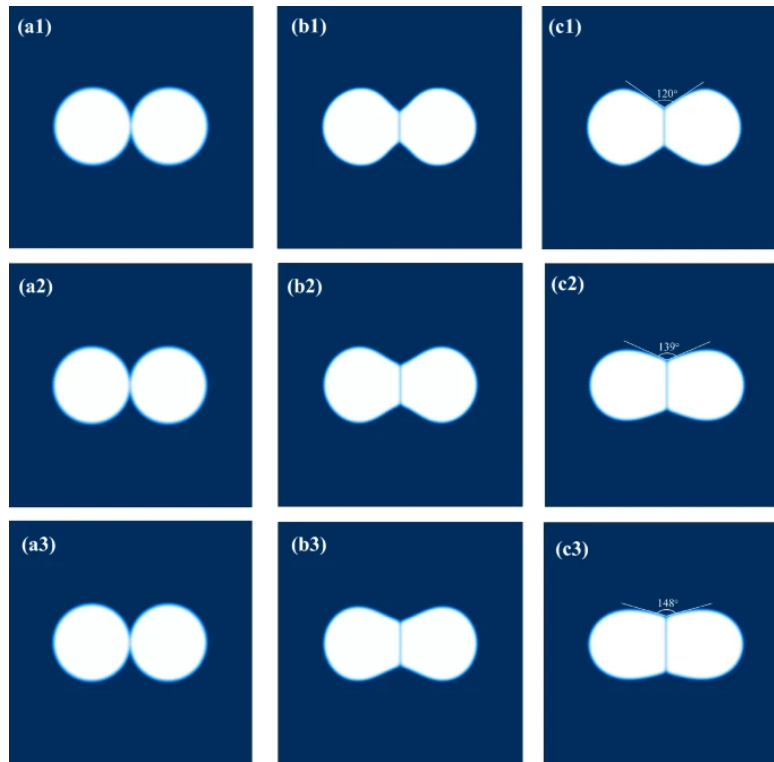


Figure 2.10: Evolution of two equal-sized silver particles under isothermal sintering of 400 °C for different times [52]

Figure 2.10 shows the PF method is widely used to study the grain merging and phase interface evolution of silver particles during sintering. The figure shows the evolution of two silver particles of the same size at different stages of isothermal sintering at 400°C. As the sintering time increases, the particles gradually fuse to form a stable bonding area, and the change in interfacial energy can also be intuitively presented through phase field simulation [19].

2.5. Shortcomings and Challenges of Current Research

Although silver sintering materials have shown great potential in the field of high-temperature electronic packaging, current research still faces some challenges that need to be addressed. During high-temperature, high-power continuous operation, microstructural changes in sintered silver or copper layers (including grain growth, pore evolution, etc.) may affect the long-term reliability of the material. For example, grain size affects the electrical, thermal and mechanical properties of the material, and the evolution of pores can lead to stress concentration and ultimately failure. [19]. In addition, silver migration is very common in high-temperature environments, increasing the risk of electrical short circuits[33]. Understanding mechanisms such as grain growth and pore evolution is a prerequisite for controlling microstructural evolution and performance in material design and application.

Although traditional experimental methods can provide some information on microstructural evolution, their high cost, long time, and inability to obtain accurate data at certain microscales make it difficult to rely on experimental methods to meet the needs of predicting the long-term aging behavior of materials. At present, there is a lack of simulation methods for

the co-evolution of pores and grain structures on a long-term scale to assist in the prediction of microstructure and reliability during thermal aging.

2.6. Choice of Methods and Their Advantages

In this section, I will explain the reasons for selecting specific experimental and simulation methods for this study.

First, EBSD was selected as a characterization tool because it is able to provide detailed information about crystal orientation, grain boundaries, and phase distribution in sintered silver materials, which is crucial for understanding microstructural changes during sintering and aging [8, 20]. In addition, EBSD can be integrated with SEM for surface analysis, providing complementary insights into surface morphology and crystal structure.

For simulations, I chose a combination of KMC and PF models to study the microstructural evolution of silver during sintering. The KMC method is well suited to understand the dynamics of the sintering process. However, it is limited in its ability to capture long-range interactions and larger-scale microstructural changes. Meanwhile, the phase field method excels in simulating the continuous evolution of phase interfaces over time. By combining KMC with the PF method, the subtle evolution of phase interfaces can be tracked while simulating grain growth, which has unique advantages in studying complex multiphase microstructures and long-term dynamic processes. [29].

These methods were chosen because they provide a detailed and multi-scale understanding of microstructural changes in sintered silver, which is critical for optimizing the performance and reliability of semiconductor packaging materials.

3

Experimental Procedures and Microstructure characterisation

3.1. Experiment Design and Fabrication Process

3.1.1. Design of Experiment

DOE (Design of Experiments) is a systematic statistical method for planning, executing, analyzing and interpreting experiments in order to obtain as much information as possible with as few experiments as possible. Its core purpose is to explore the relationship between dependent variables and independent variables in an organized way to optimize the process[41]. It is very important to control the independent variables of the experiment. In this experiment, there are many independent variables and it is impossible to test them one by one. After reading a lot of literature and careful analysis, partial factor experiments were decided to reduce the number of experiments.

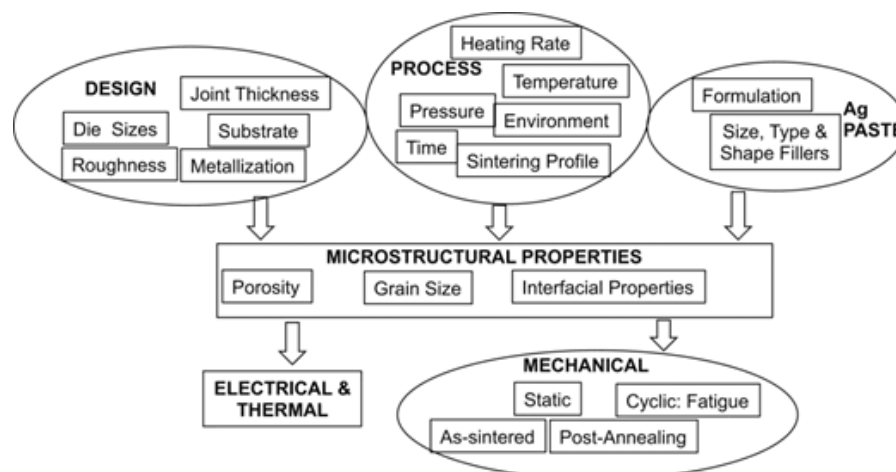


Figure 3.1: Influence of the input factors (i.e., design, process and Ag paste formulation) on the microstructural properties (i.e., porosity, grain sizes, and interfacial properties) and the resulting mechanical, electrical and thermal properties of the sintered Ag joint[45]

As shown in **Figure 3.1**, the performance of sintered silver is related to many factors.

Design factors such as solder joint thickness, chip size, roughness, substrate, etc. cannot be changed well, so we fix the basic performance such as size; we choose the copper substrate size of 10 mm×20 mm×1 mm, the chip size of 1 mm×5 mm×0.14 mm, and the thickness of the sintered silver bar of 40µm.

Pure silver is selected as the main material because compared with alloy silver materials, pure silver has better chemical stability, higher sintering density, more stable performance at high temperature, and no harmful intermetallic compounds. At the same time, pure silver prevents other organic residues and ensures purity. In addition, pure silver materials are more environmentally friendly.

Process parameters including heating rate, temperature, pressure, sintering time and atmosphere will affect the microstructure. The sintering method is pressureless sintering, and the heating rate and sintering time are fixed. The sintering process takes into account different atmospheres, like Air, Nitrogen, and Nitrogen with Formic Acid Vapor, which are common sintering atmospheres in the industry. The aging process takes into account different atmospheres (Air, Nitrogen) and temperatures (200 °C, 250 °C). These factors determine the characteristics of the material's microstructural properties, which in turn affect the electrical, thermal, and mechanical properties of the device.

3.1.2. Sample Preparation

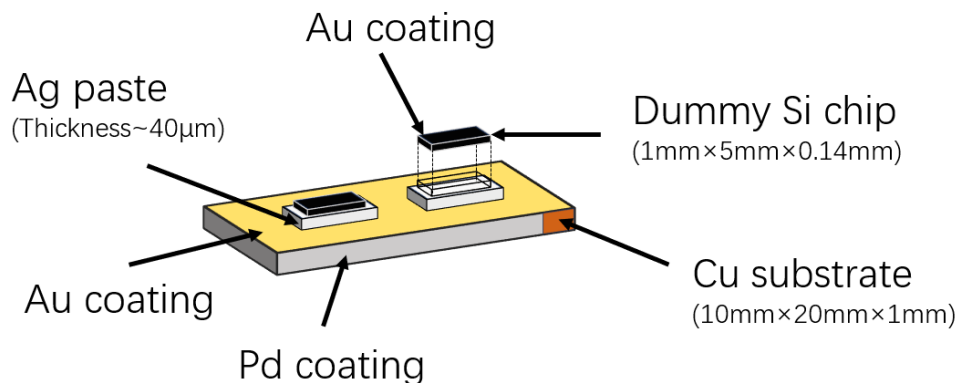


Figure 3.2: schematic of the device structure

Figure 3.2 shows an electronic packaging structure, in which the virtual silicon chip is connected to the copper substrate through a layer of silver paste, and the thickness of the silver paste is about 40 µm. The entire surface of the copper substrate is plated with a palladium layer. A thin layer of gold is also plated on the surface of the chip, mainly to ensure a firm connection and conductivity. The entire packaging design aims to achieve efficient mechanical support, electrical conductivity, and thermal conductivity through the silver paste and to ensure the stability and reliability of the chip in a high-temperature and high-power environment.

The white X pattern in the picture is Ag paste. It is applied to the copper substrate in an X pattern, and then the die is placed on it to form the sample that will be sintered later. The

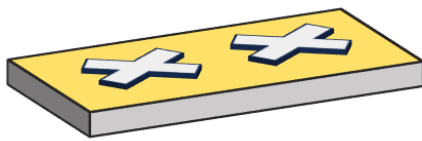


Figure 3.3: Schematic diagram of sintering silver paste position

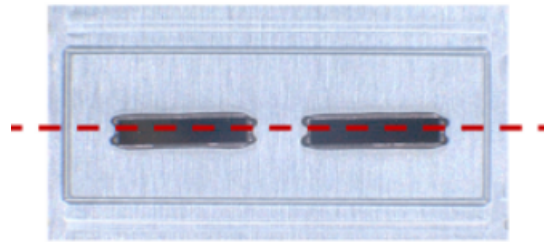


Figure 3.4: Top view of sample

picture below is the top view of the sample. The red line in the picture is the position where plan to check the cross-sectional interface.

3.1.3. Low-Temperature sintering & Aging Experiment

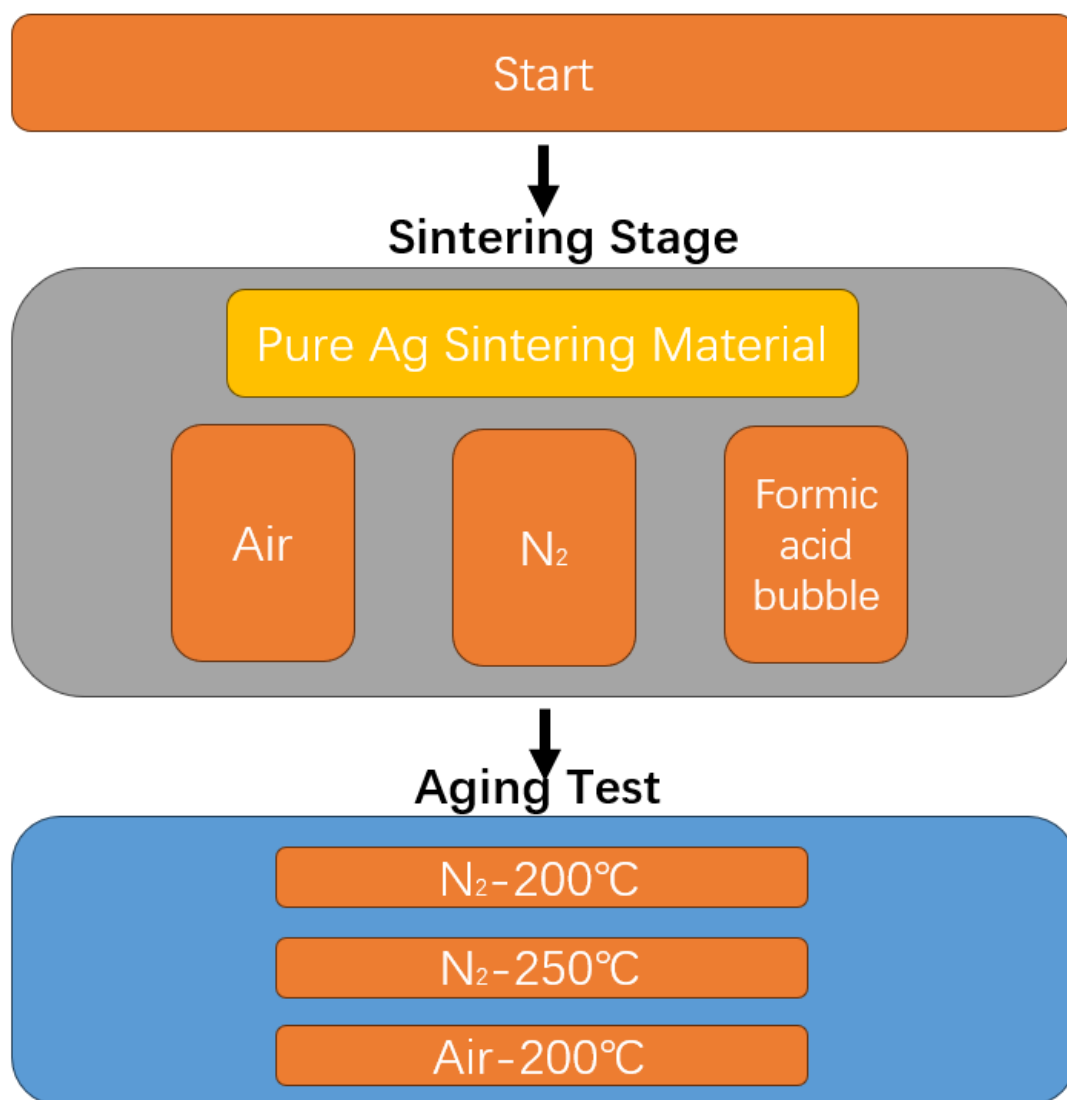


Figure 3.5: Flowchart of sintering and aging processes

Next comes the key steps of sintering and aging. In terms of the choice between pressure and pressureless sintering, pressureless sintering has many advantages over pressure sintering. First, it does not require external pressure, avoiding mechanical damage to brittle materials such as silicon chips. Second, the process is simpler, the equipment cost is lower, and the production efficiency is improved.

Sintering and Aging Condition

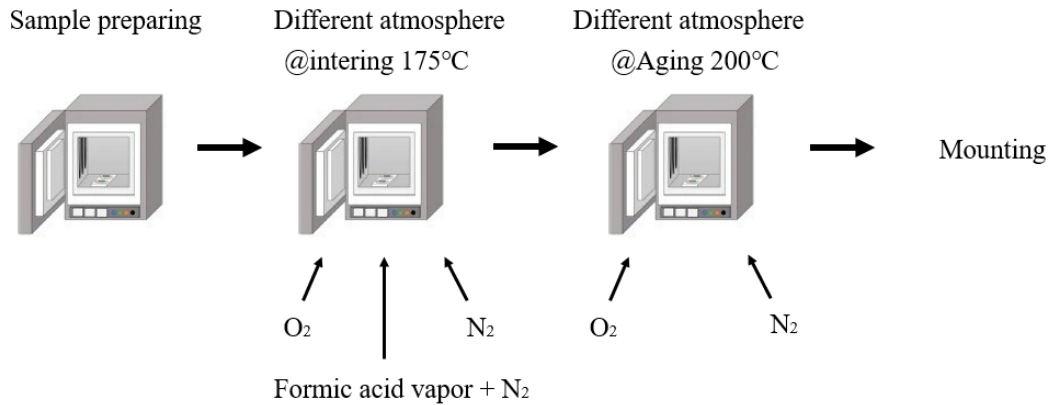


Figure 3.6: Schematic diagram of sintering and aging treatment processes under different atmospheres

Figure 3.6 shows a sample processing flow, including sample preparation, sintering in different atmospheres, and aging treatment in different atmospheres. The atmosphere of the sintering and aging process can be selected as oxygen or nitrogen, which affects the performance of the sample. After the treatment is completed, the sample enters the mounting stage for material characterization.

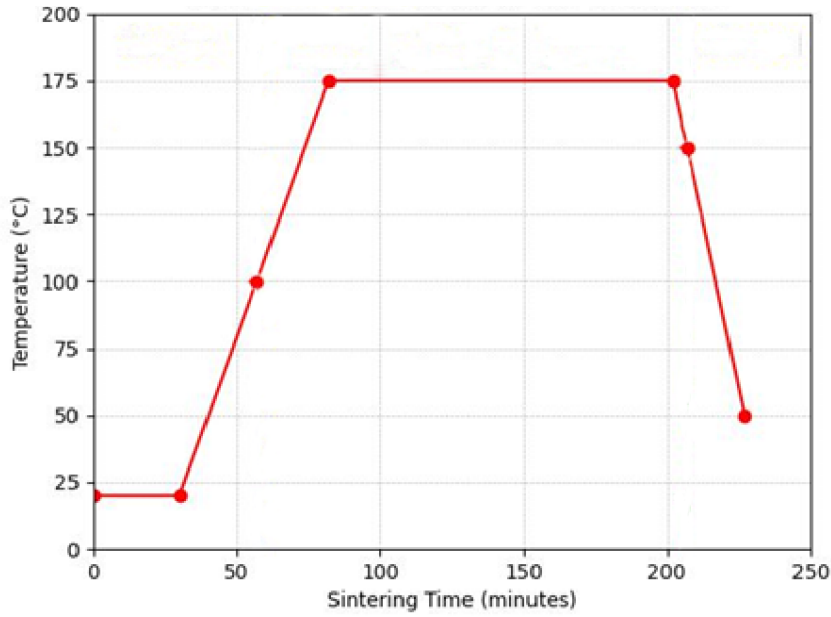


Figure 3.7: Temperature variation over time during sintering

Figure 3.7 shows the change of temperature over time during the sintering process, reflecting the specific characteristics of the heating rate and heating time. First, the temperature rises rapidly from about 25 °C to 175 °C. The entire heating process lasts for about 50 minutes, and the heating rate is about 3 °C per minute. After reaching 175 °C, the temperature remains constant between 50 minutes and 200 minutes. This long constant temperature stage helps to ensure sufficient sintering and densification of the material. After 200 minutes, the temperature drops with around 5 °C per minute, the sintering process ends and enters the cooling stage and subsequent aging stage.

Classify Different Aging and Sintering Conditions on Different Time Scales

Test	Ageing Condition	0Hr	1Week[168hrs]			3Week[504hrs]			6Week[1008hrs]		
		Sintering Condition	E	F	G	E	F	G	E	F	G
L1	in Air, 200C	E:Sintering in O2 condition	L1E168	L1F168	L1G168	L1E504	L1F504	L1G504	L1E1008	L1F1008	L1G1008
L3	in N2, 200C	F:Sintering in N2 condition	L3168	L3F168	L3G168	L3E504	L3F504	L3G504	L3E1008	L3F1008	L3G1008
L4	in N2, 250C	G:Sintering in formic acid	L4168	L4F168	L4G168	L4E504	L4F504	L4G504	L4E1008	L4F1008	L4G1008

Table 3.1: Experimental sintering and aging conditions diagram

Table3.1 records all the experiments I prepared in different atmospheres and on different aging time scales. The samples with test numbers L1, L3, and L4 were aged at high temperatures in air and nitrogen environments, respectively. Among them, the L1 sample was aged at 200°C in air, the L3 sample was aged at 200°C in nitrogen, and the L4 sample was aged at 250°C in nitrogen. At 0 hours, three flanges were sintered under different sintering conditions, including Oxygen sintering (E), Nitrogen sintering (F), and sintering under Nitrogen with formic acid vapor conditions (G). The test time points are divided into 1 week (168 hours), 3 weeks (504 hours), and 6 weeks (1008 hours), and each time period corresponds to the records under different sintering conditions. Through these data, we can analyze how the microstructure and properties of the samples change over time under different sintering and aging environments so as to evaluate their long-term stability and reliability in high-temperature environments.

Mounting

After sintering, the sample needs to be cold mounted. Cold mounting is a technique to embed the sample in resin at room temperature, which is suitable for preparing samples that are processed at low temperature and low pressure. First, the sample needs to be cleaned and selected a suitable mold, then fixed with a holder before mounting.



Figure 3.8: Mounting diagram

Then put ClaroCit Powder and ClaroCit Liquid into the mold, mixed in the ratio of 2 Powder: 1 Liquid to ensure that the sample is completely covered by the resin. In order to observe the sample, the sample after mounting needs to maintain a high degree of transparency, but this will cause the sample to be wrapped by polymer powder and thus non-conductive, which will also bring some troubles to the subsequent experiments. Then put it in the pressure cooker and let it stand for 20 minutes to wait for the polymer to solidify, then the sample can be polished for observation and analysis.

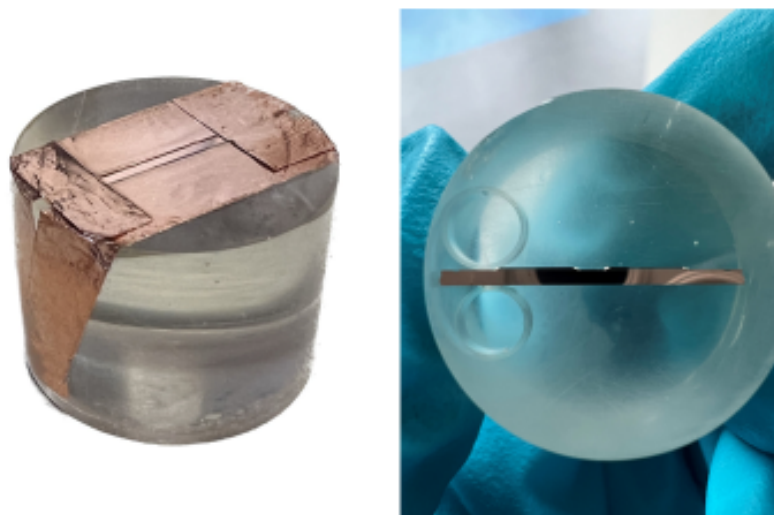


Figure 3.9: Schematic diagram of cross-sectional sample

The cross-sectional sample are depicted in **Figure3.9**.

3.2. Shear Test

3.2.1. Experimental Preparation

Shear test plays an important role in studying the bonding strength and reliability of sintered materials. It is applied to evaluate the effect of different sintering parameters (such as temperature, pressure, time, heating rate, etc.) on the strength of silver paste.

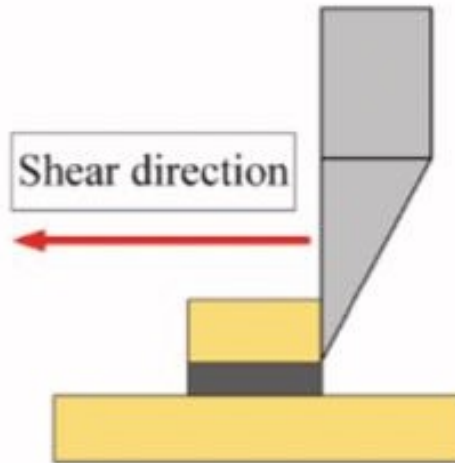


Figure 3.10: Shear direction test diagram

The **Figure 3.10** shows the process and principle of the shear test. The actual shear test equipment is a metal tool head that contacts the sample vertically, and the sample is fixed on the fixture. The tool head applies a shear force in the horizontal direction, with the purpose of testing its strength by shearing the sample. The second picture is a schematic diagram of the principle of the shear test, showing how the shear tool applies force in the horizontal direction to cut the sample off from the bonding interface. The test determines the shear resistance of the material by applying a gradually increasing horizontal force until the sample or the bonding layer fails.

Parameter	Value
Test Speed	200.0 $\mu\text{m/s}$
Shear Height	20.0 μm
Test Load	0.50 kg
Bonder	Shear Tool 5.6 mm

Table 3.2: Key parameters from the shear test

The shear test consists of four main parameters: the test speed, measured at 200.0 $\mu\text{m/s}$; the shear height, set at 20.0 μm ; the applied test load of 0.50 kg; and the specifications of the bonding machine, which uses a shear tool with a diameter of 5.6 mm.

3.2.2. Analysis of Maximum Load Force Variation Under Different Aging and Sintering Conditions

To explore the shear strength under different atmospheres and time scales, the discussion is divided into two groups: L1E/L3E (different aging atmospheres at 168h, 504h, 1008h) and L1E, L1F, L1G (different sintering atmospheres at 168h, 504h, 1008h). There are three or four samples under each different condition, and after obtaining their Maximum Load Force, the average value is obtained and the graph is made.

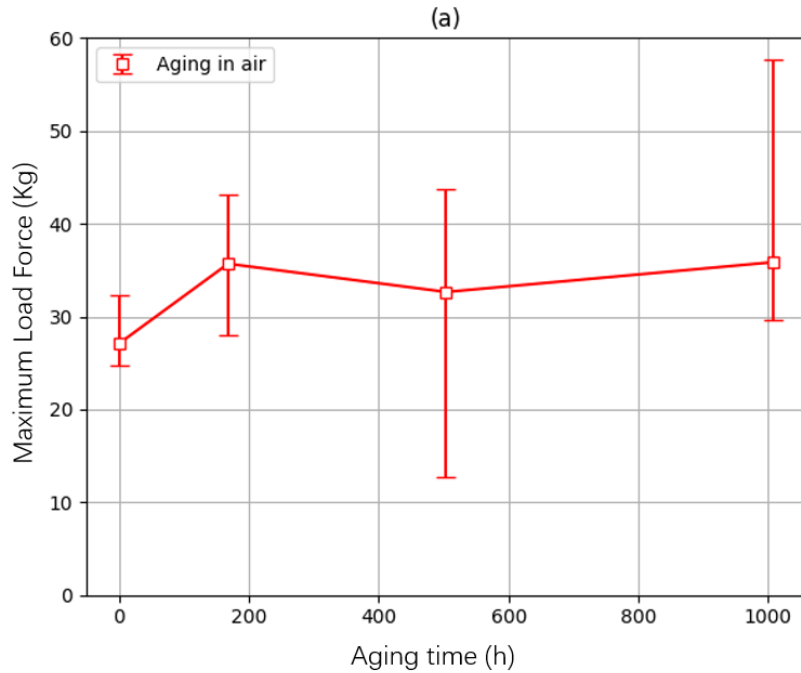


Figure 3.11: Relationship between aging time and maximum load force aging in an air environment

Figure 3.11 shows the effect of air aging, air sintering at 200°C process (L1E) on shear strength. The horizontal axis represents the aging time and the vertical axis represents the maximum load force. It can be seen that with the increase of aging time, the average value of maximum load force does not show an obvious trend fluctuation. However, compared with the sample of 0 hours, the overall maximum load force of oxidation in air has increased. At around 168 hours, the maximum load force reaches a peak of about 40 kg, after which the maximum load force decreases slightly. At 1008 hours, the maximum load force increases slightly again.

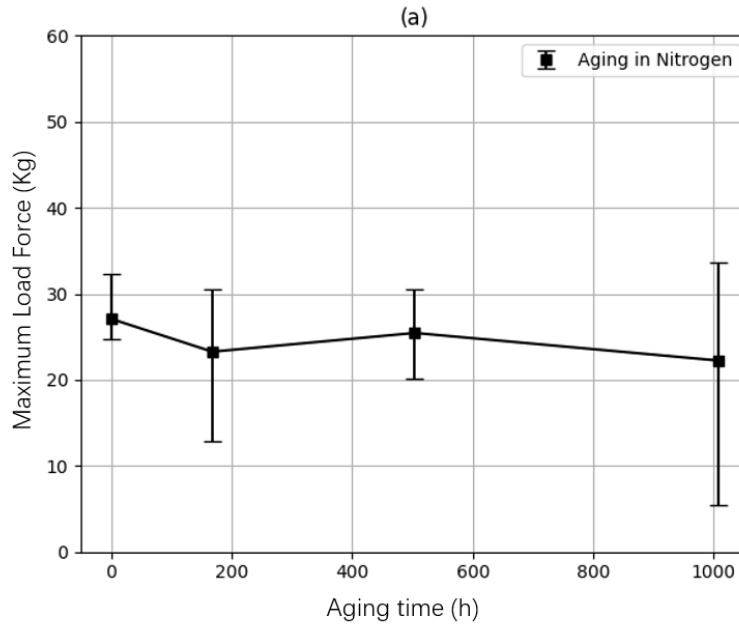


Figure 3.12: Relationship between aging time and shear strength in a nitrogen environment

Figure 3.12 shows the effect of nitrogen aging, air sintering at 200 °C process (L3E) on maximum load force. As can be seen from the figure, with the increase of aging time, the maximum load force decreases slightly overall, but the change is not significant. At 0 hours, the maximum load force is about 30 Kg, and then it decreases slightly around 168 hours, close to 25 Kg. After that, in the 504 hour range, the maximum load force rebounds to about 30 Kg, but it drops slightly again to about 23 Kg at 1000 hours.

In general, the maximum load force of aging in a nitrogen environment changes less with time and has less volatility; the maximum load force of aging in air has greater volatility and poorer stability. This is mainly because nitrogen, as an inert gas, can effectively inhibit the oxidation process of sintered silver materials. When aging in a nitrogen environment, the maximum load force decreases with time but increases in air. This is because the decrease in the maximum load force during aging in a nitrogen environment is due to the accumulation of microscopic defects, while the increase in the maximum load force in the air is due to the surface hardening effect formed by the oxidation reaction[26], but it still a temporary phenomenon.

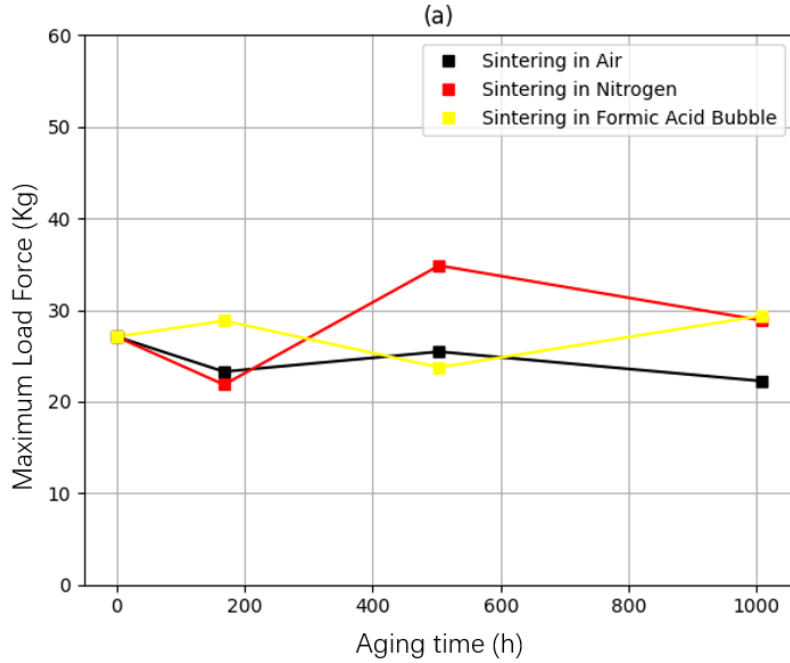


Figure 3.13: Variation of shear strength with aging time under different sintering conditions

Figure 3.13 shows the maximum load force variation trend of sintering in different atmospheres (air, nitrogen and formic acid vapor). At 168h, it can be seen that the maximum load force of the material sintered in formic acid vapor is the highest. This is because formic acid produces a reducing atmosphere during the sintering process, which can effectively remove oxides in the material and promote particle densification and interface bonding. At the same time, since oxides are more easily formed in air, the sintering strength is the lowest. At 504h, a reversal occurred, and the maximum load force sintered in nitrogen was the highest. The reason for this phenomenon here may be that the average value is prone to errors. At 1008h, the shear strength of sintering in formic acid vapor returned to the highest. Overall, sintering in formic acid bubbles tends to remove oxides, thereby improving the strength of the material. The average load force for each sintering condition is as follows:

- **Sintering in air:** 26.3 kg
- **Sintering in nitrogen:** 32.1 kg
- **Sintering in formic acid vapor:** 30.8 kg

3.2.3. Fracture Position Check after Sheer Test by SEM

After analyzing the shear strength trend of the complete body, the microstructure of the surface needs to be analyzed, which helps to understand the failure mechanism of the material. Through this analysis, the microscopic defects in the material are observed, analyze the thermal fatigue of the material, and better analyze how to improve the mechanical properties of the material and extend the life of the material.

Pure Ag sintering material @ Sintering in Air @ Thermal Aging under 200C_Air

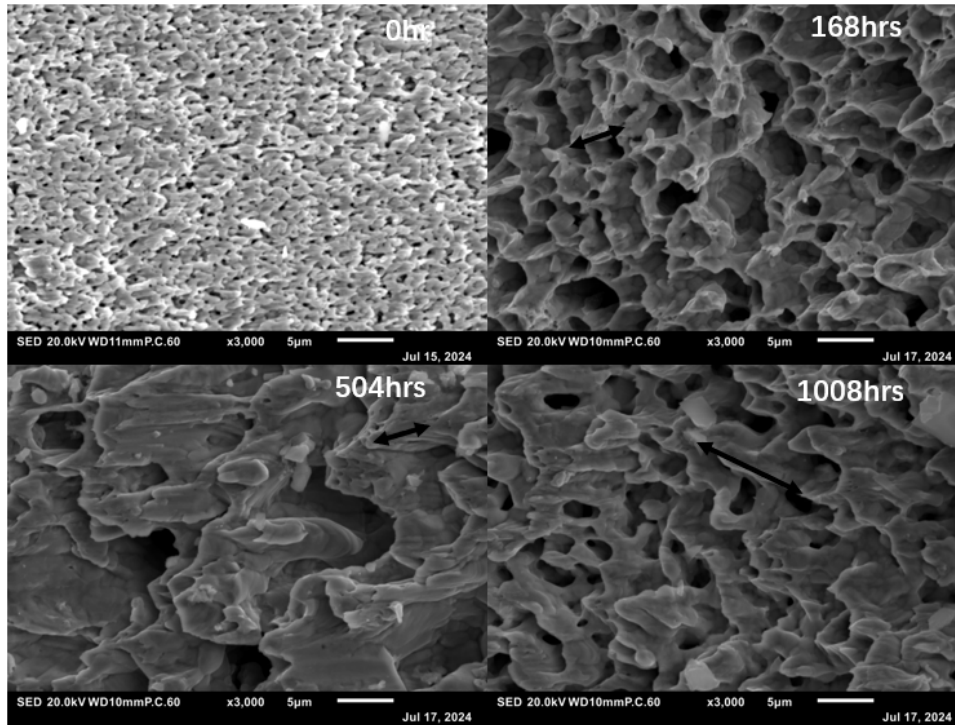


Figure 3.14: Thermal aging microstructure evolution of pure silver aging at 200°C in air environment

Figure 3.14 shows the microscopic fracture surface structure of pure silver sintered material in an air environment at 200°C with aging time (LIE), with a magnification of 3000X and a scale of 5µm. At 0 hours, the fracture surface of the material is dense and uniform, with low porosity, indicating good mechanical properties; after aging to 168 hours, holes begin to appear on the surface, the structure becomes loose, and the porosity increases; at 504 hours, the holes further expand, indicating that the material structure is even looser; after 1008 hours, the holes expand more, indicating that the material has deteriorated and the strength has decreased. At the same time, according to the arrows marked in the figure, that is, the tip length of the dimple fracture, it can be found that from 0 hours to 504 hours, the length of the dimple fracture is constantly increasing, which also means that the material has better and better toughness. Corresponding to **Figure 3.13**, it can be found that the maximum load force has an upward trend. However, after 1008 hours, the length of the dimple fracture has decreased, which means that the toughness of the material has decreased, and the maximum load force has also decreased accordingly. There are many reasons for this phenomenon. When aging in the air, the oxide layer formed on the surface of the material plays a protective role in the early stage, improving the mechanical properties because the dense oxide layer increases the surface hardness and corrosion resistance. However, as the aging time increases, the oxide layer gradually becomes thicker and more brittle, prone to cracks and peeling, resulting in stress concentration and material damage, thereby reducing the mechanical properties. Therefore, it is not that aging in an anaerobic environment is beneficial to the material, nor is it that aging in an aerobic environment is good. There must be an Oxygen ratio that allows the mechanical properties of the material to reach the best. In an oxygen environment, the best mechanical properties are achieved after aging for 504h, and then they will decline. However, in other

environments, it may take a longer time to achieve the best mechanical properties.

Pure Ag sintering material @ Sintering in Air @ Thermal Aging under 200C_N2

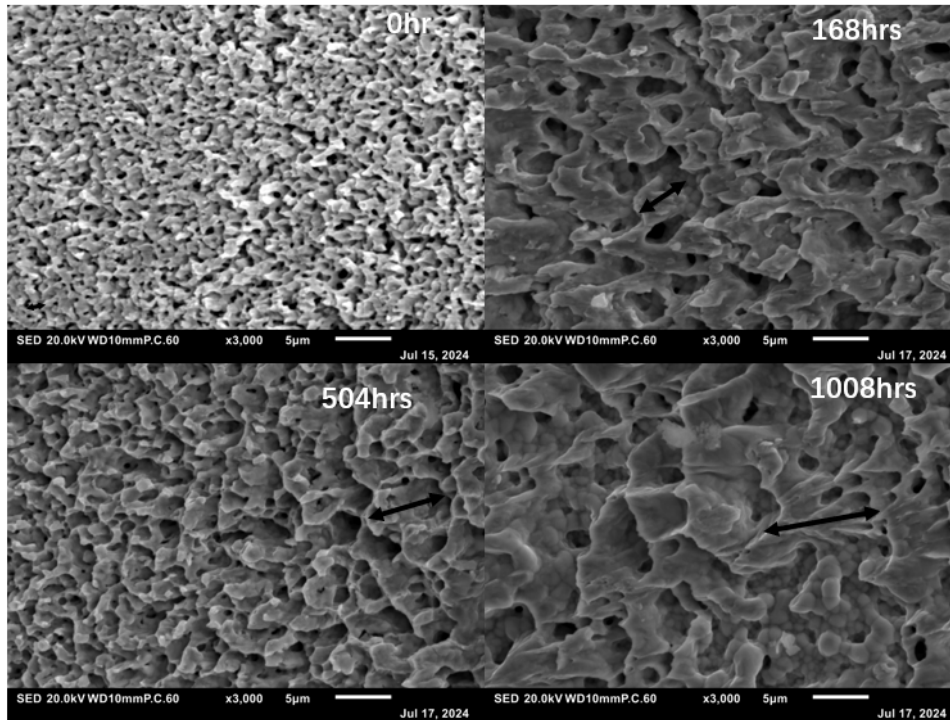
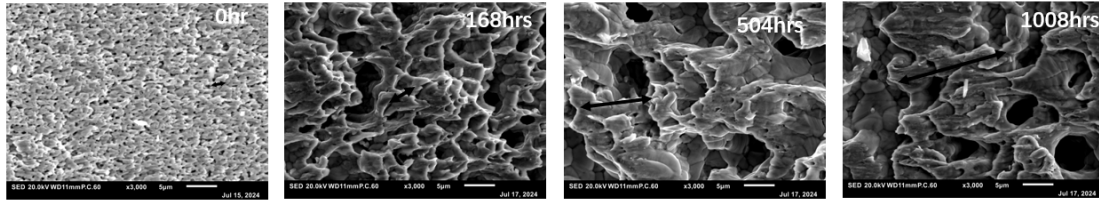


Figure 3.15: Thermal aging microstructure evolution of pure silver aging at 200°C in nitrogen environment

Figure 3.15 is a microstructure diagram (L3E) of pure silver material changing with time during thermal aging at 200 °C in a nitrogen environment. The magnification is 3000X, and the scale is 5µm. At 0 hours, the surface of the material is dense and uniform, but with the increase of aging time, holes begin to appear after 168 hours, and the number of holes increases further after 504 hours, and the structure becomes irregular. By 1008 hours, the cracks have obviously expanded, and the number of holes has increased significantly, indicating that the internal degradation of the material has intensified. Observing the tip length of the dimple fracture, it can be found that the length of the dimple fracture has abnormally decreased since 504 hours, but observing **Figure 3.13**, it is found that the maximum load force is increasing, indicating that the toughness of the material has improved. However, after 1008 hours, the length of the dimple fracture has increased, which means that the toughness of the material has increased again, but the maximum load force has decreased. This phenomenon may occur because the position of the dimple fracture observation has shifted.

In general, with the increase of aging time, the material structure deteriorates, the pores expand, and the mechanical properties and shear strength gradually decrease in theory. Although the nitrogen environment inhibits oxidation, long-term high temperatures will still cause irreversible structural damage.

Pure Ag sintering material @ Sintering in N₂ @ Thermal Aging under 200C_Air



Pure Ag sintering material @ Sintering in FA @ Thermal Aging under 200C_Air

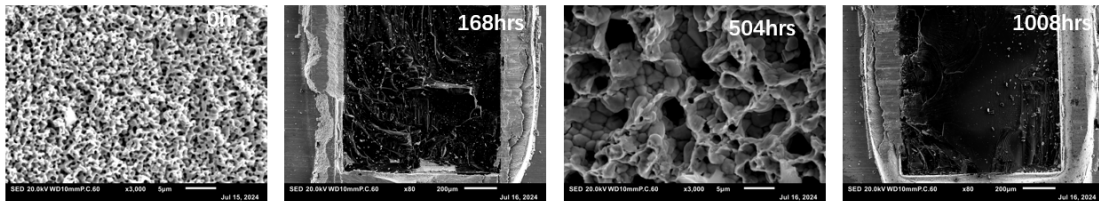


Figure 3.16: Thermal aging microstructure evolution of pure silver aging at 200°C in air environment with different sintering condition

Figure 3.16 shows the microstructure of pure silver material sintered in nitrogen and formic acid vapor (L1F/L1G) during heat aging at 200 °C in nitrogen environment. The magnification is 3000X and the scale is 5µm. It can be observed from the figure that the length of the dimple fracture increases longer, which means that the material can absorb more energy during plastic deformation and show higher toughness. Even the 168h and 1008h of the sample sintered in Nitrogen with formic acid vapor(L1G) did not destroy the upper Si layer, indicating that the material has good toughness.

3.3. Microstructure Evolution Analysis During Aging Tests

After observing the results of the shear test, further characterization work is needed to explore the underlying mechanism.

3.3.1. Cross-sectional Images by FIB

FIB(Focused Ion Beam)-SEM is a technique that uses high-energy ion beams to precisely process and image samples. FIB is often used in conjunction with SEM to cut materials at nanometer precision.

FIB is important for observing microstructures because it can precisely remove the surface layer of the material, expose the internal structure, and obtain the microscopic morphology of the material. At the same time, the cross-section prepared by FIB can be directly imaged by SEM.

Samples Ageing in Nitrogen(L3)

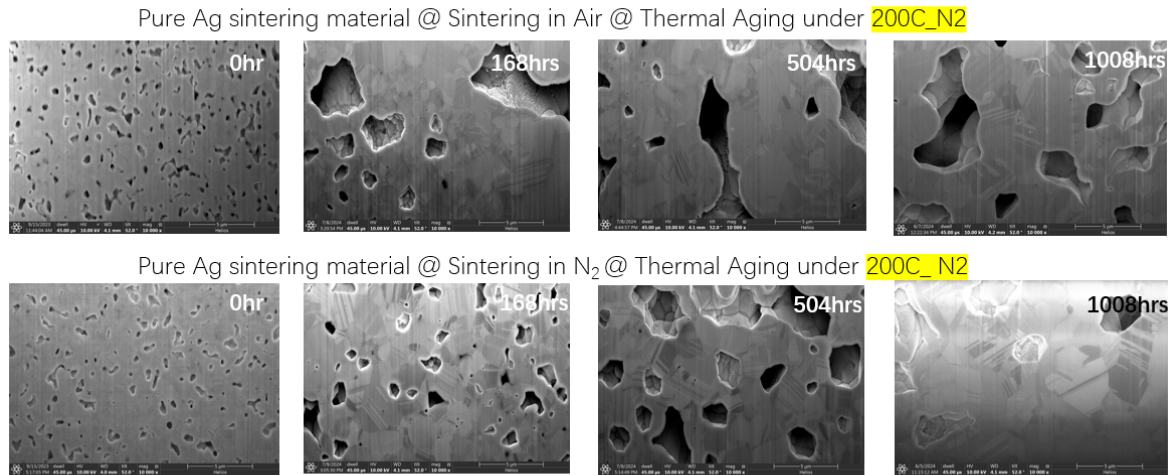


Figure 3.17: Comparison of microstructures of pure silver sintered materials at 200°C in air and nitrogen environments after thermal aging in nitrogen

This set of images shows the evolution of the microstructure of the sintered in air (L3E) and nitrogen (L3F) at 200°C in a nitrogen environment for different aging times (0 hours, 168 hours, 504 hours, 1008 hours). The images show the cross-section of the material, and the evolution of the pores can be clearly observed.

It can be found that the internal pores of this material at 0 hours are smaller and evenly distributed. Although the number of pores is greater, their size is smaller, indicating that the microstructure of the material is relatively dense at this time, and therefore the mechanical properties are maintained well. After 168 hours of aging, the pores inside the material increase, and the mechanical strength may begin to decrease. By 504 hours, the pores further enlarged, and some pores became deeper. Finally, after 1008 hours of aging, the number and size of holes increased significantly, and some holes were even connected to each other. The entire cross-section looks very loose and irregular, showing that the material has deteriorated, and the internal structure has lost its density.

As the material ages, not only can the expansion of pores be observed, but also the formation of precipitates around some pores can be noticed. The formation of such precipitates is usually caused by local segregation or redistribution of the material, resulting in the deposition of some enriched phases around the pores. Such precipitates are also likely to be caused by impurities or other trace elements in silver migrating and depositing at the pore boundaries during heat treatment. On the one hand, the pores themselves have reduced the strength and durability of the material; on the other hand, the presence of precipitates may cause the areas around the pores to become more brittle. These areas may be more likely to become the starting point of cracks, which in turn leads to a decrease in mechanical properties[12].

A lateral comparison shows obvious differences in sintering in air (L3E) and sintering in nitrogen (L3F). Due to oxidation, the pores of the material sintered in air expand faster, the pore size is large and irregular, and there are more precipitates, which leads to faster material degradation. In contrast, materials sintered in nitrogen have slower pore expansion, smaller

and more regular pores, less precipitated phases, and a more stable overall structure because the inert gas inhibits the oxidation process. Therefore, materials sintered in nitrogen have better durability under high-temperature aging conditions.

Samples Ageing in Air(L1)

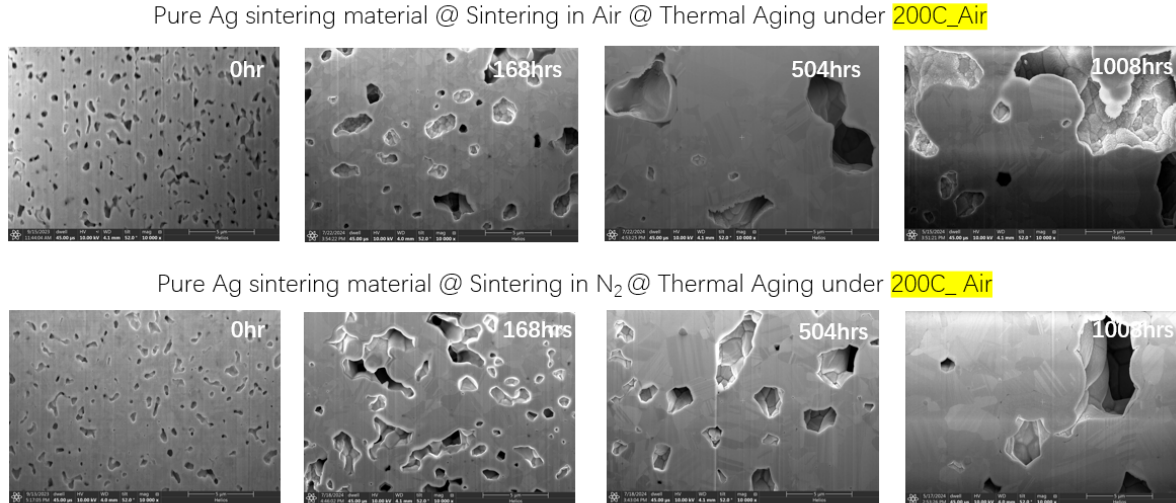


Figure 3.18: Comparison of microstructures of pure silver sintered materials at 200°C in air and nitrogen environments after thermal aging in air

Materials aging in air showed more pores and more irregular pore shapes than those aged in a nitrogen environment. Due to the influence of oxidation, the number and size of pores increased significantly, especially after long-term aging (504 hours and 1008 hours), the pores became more irregular and larger.

3.3.2. Comprehensive Microstructural Analysis Using EBSD

Electron backscatter diffraction plays an important role in observing the microstructure of sintered silver materials. It can provide key information such as grain size, crystal orientation, stress distribution, etc. The analysis of these microstructures is of great significance for optimizing the sintering process and improving material properties.

Sample Preparation

Before conducting EBSD, sample preparation is also very important. The sample needs to be tilted at an angle of about 55° when performing EBSD, and the maximum sample thickness of the holder placed in the chamber cannot exceed 5 mm. However, when mounting the sample, the thickness of the sample is about 15 mm, and the sintered silver layer has not been completely exposed, so mechanical grinding and mechanical polishing are required at this time, followed by ultrasonic cleaning to remove contaminants, drying and storing in a clean environment, and finally ion milling of the sample is required. The key is to obtain a smooth, contamination-free surface to ensure a clear diffraction image for crystallographic analysis.

After the initial attempt at EBSD, some problems occurred. As mentioned above, the polymer powder used is not conductive, which causes the resin area to be charged and causes image

drift. So we had to re-grind until the bottom was penetrated and the entire sample was transparent. Then a layer of copper tape was wrapped around the sample, exposing only the sintered silver layer that needed to be observed. After observation, it was found that charging of the sample is avoided by touching direct contact of the metal sample and the use of Cu tape.



Figure 3.19: Thinned sample wrapped with copper tape

Grain Orientation Analysis through EBSD

Inverse Pole Figure (IPF) is an image generated by EBSD and is used to analyze the grain orientation in the material microstructure. It displays the orientation of the grains in color coding, with black lines representing grain boundaries, red lines representing twin boundaries, and black arrows representing the location of the holes. IPF is important for evaluating the anisotropy, mechanical properties, and crystallographic characteristics of the material, and can better help me understand the microstructure evolution during the aging process.

Pure Ag sintering material @ Sintering in Air @ Thermal Aging under 200C_Air

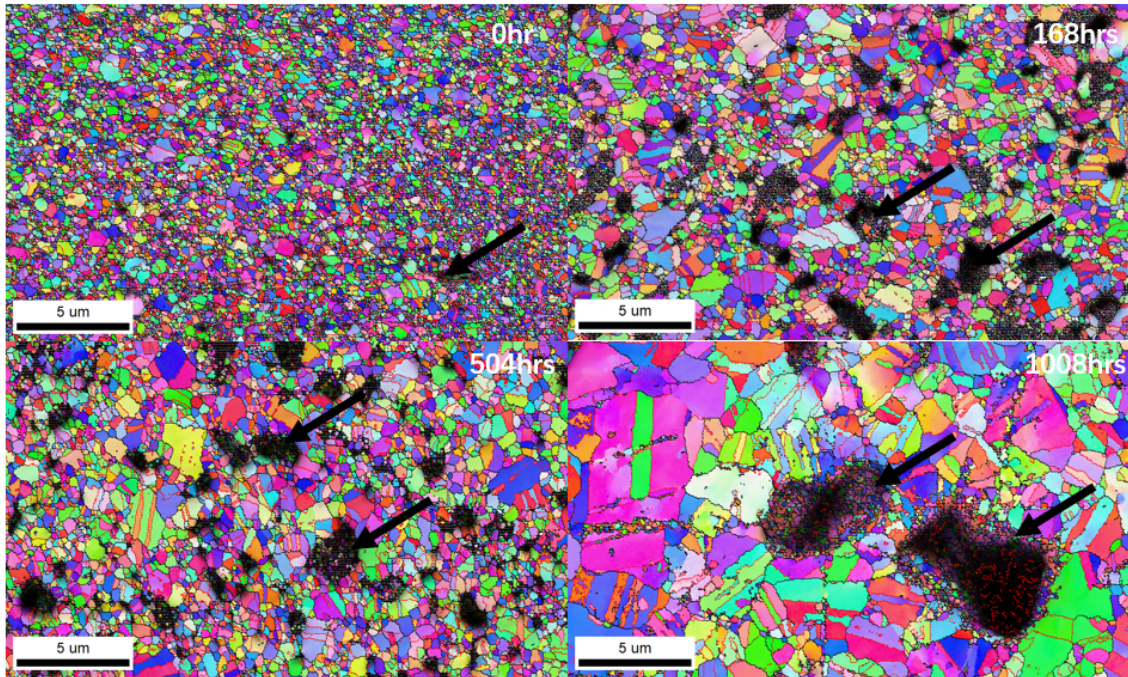


Figure 3.20: Inverse Pole Figure of thermal aging of pure silver sintered material at 200°C in air environment

Figure 3.20 shows the microstructural changes of the material aging in air (L1E). From the 0 hour image, it can be seen that the grain size of the material is small and evenly distributed, with dense grain boundaries and uniform twin distribution. In the 168-hour image, holes and defects gradually increased, and the grain boundaries in some areas began to change slightly, but the overall grain structure remained relatively intact. After 504 hours, the number of pores increased significantly, the holes and defects shown in the black area expanded, and the grain boundaries became more irregular. At the same time, the distribution of twins becomes more sparse. By 1008 hours, significantly larger holes and defects can be seen in the image, the irregularity of the grain boundaries intensifies, the grains become coarser and irregular in shape, and the number of twins is also significantly reduced.

These phenomena show that during the long-term aging process at high temperature, the pores and defects inside the material gradually increase, the grain size continues to increase, and the twins continue to decrease, which indicates that the mechanical properties of the material have significantly declined.

Some grains will be formed during the sintering process, and twins will be generated because the grain size is larger than the Ag NPs size. Twins help to enhance the plasticity and toughness of the material, especially under high temperature or large deformation conditions. It can promote the ductility and impact resistance of the material, but it does not mean that the more twins, the better the mechanical properties of the material.

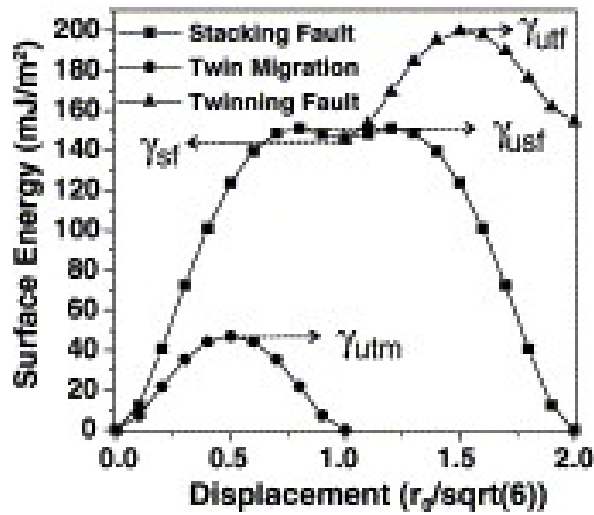


Figure 3.21: Surface energy variation with different defect mechanisms[13]

A. Frøseth et al. analyzed the surface energy changes associated with different defect mechanisms, including stacking faults, twin migration, and twin stacking faults. This figure depicts how the surface energy changes with displacement, and the overall trend is found to be a normal distribution[13].

Pure Ag sintering material @ Sintering in Air @ Thermal Aging under 200C_ N₂

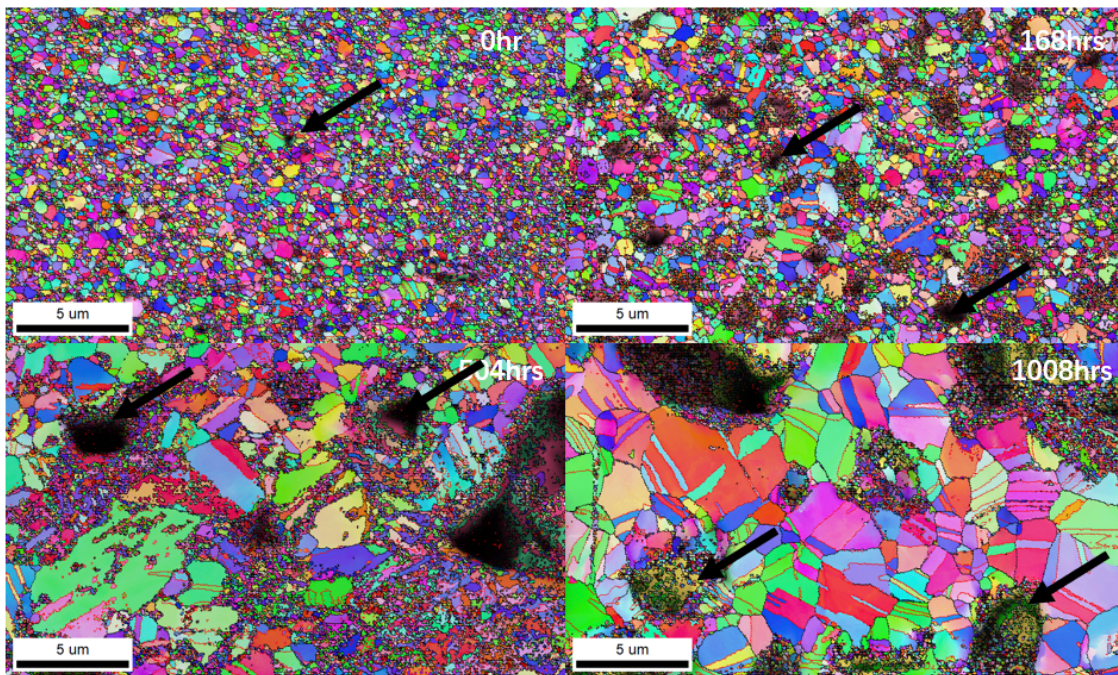


Figure 3.22: Inverse Pole Figure of thermal aging of pure silver sintered material at 200°C in Nitrogen environment

This Figure3.22 shows the thermal aging process of the material at 200°C (L3E) in a nitrogen environment. As the aging time increases, pores and defects gradually increase and expand,

the grain structure gradually becomes irregular from the initial small and uniform size, and the grain size increases. Especially after 504 hours and 1008 hours, the material deteriorated significantly and the pores expanded significantly, showing the damage to the microstructure of the material caused by aging. These changes indicate that long-term high-temperature aging significantly affects the mechanical properties of the material, leading to a decrease in its strength and toughness.

Compared with aging in air, aging in nitrogen environment results in a more uniform grain size distribution, less pore and defect expansion, and better preservation of twin structure. In air environment, oxidation accelerates grain boundary migration and grain growth, resulting in uneven grain size, significantly more pores and defects, and less twinning. These differences reflect that nitrogen environment is more conducive to maintaining the structural stability and mechanical properties of the material.

Grain Size Analysis

The Grain Size diagram shows the distribution of different grain sizes within the material, helping me understand the microstructure of the material. Grain size is a key factor affecting material performance. Small grains improve the strength and hardness of the material because grain boundaries can hinder dislocation movement and crack propagation; while large grains help to improve the ductility and high-temperature creep resistance of the material, but usually reduce strength and fatigue performance.

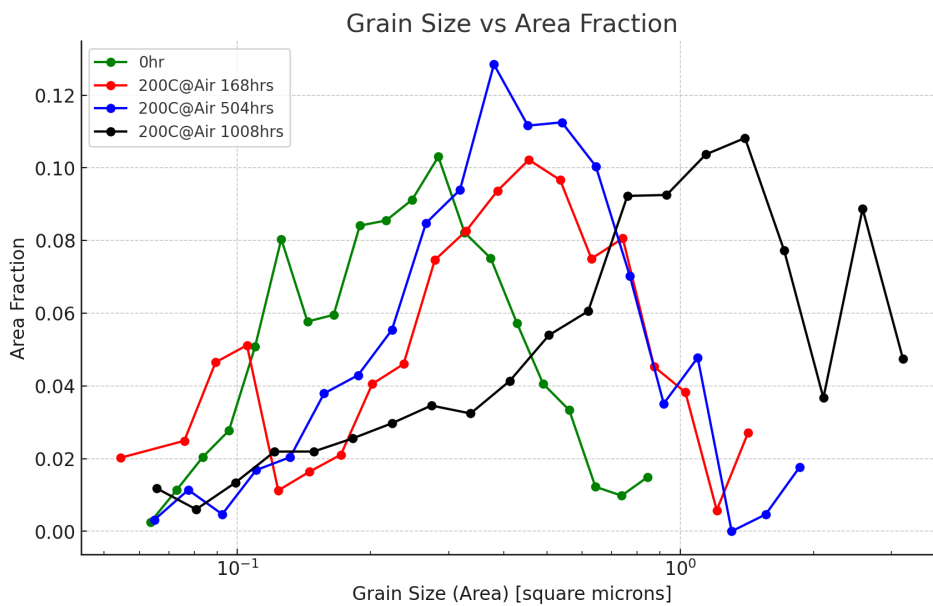


Figure 3.23: Relationship between grain size and area fraction after thermal aging at 200°C in air

Figure 3.23 shows the grain size of the material after heat aging at 200°C (L1E) in air. It can be seen from the figure that the grain size gradually increases with the aging time. In the initial state (0hr), the grains are mainly concentrated in a smaller size range, indicating that the material has higher strength and hardness. As the aging reaches 168 hours, the grains begin to grow and the distribution range becomes wider. The material strength may decrease but the ductility will also increase. At 504 hours and 1008 hours, the grain size increases further, and

large grains dominate. As the grains grow, the strength and hardness of the material gradually decrease.

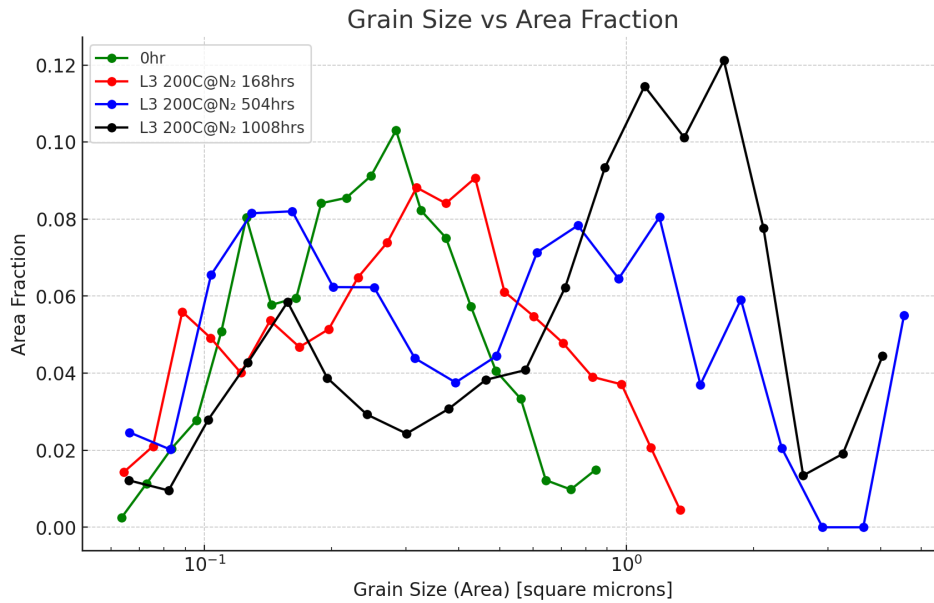


Figure 3.24: Relationship between grain size and area fraction after thermal aging at 200°C in nitrogen

Figure 3.24 shows the grain size of the material thermally aged at 200°C (L3E) in a nitrogen environment. At 0 hr, the grains are mainly concentrated in a smaller size range, indicating that the grains are smaller. By 168 hours, larger grains begin to form and the grain size increases. At 504 hours, the phenomenon of grain growth becomes more obvious, and the number of larger grains increases. When aging to 1008 hours, the area fraction of large grains increased significantly, indicating that the grains continued to grow over time. The overall trend is similar to that of L1E. As the aging time increases, the grain size continues to increase. However, the grain size diagrams of 504h and 1008h show that there are more large-sized grains. The reason here is that impurities are scanned, such as a part of copper.

Comparing the two sets of images, it is found that the grain growth of the L1 group in the two sets of images shows a more obvious peak concentration trend, and the peak appears in a larger grain size area, indicating that L1 has a larger grain size in comparison; The peak distribution of the L3 group is more dispersed, and different time curves show multiple peaks, especially in the aging time periods of 504 hours and 1008 hours.

The multiple peaks may indicate abnormal grain growth (AGG) occurring during the aging process of the material. AGG usually refers to the phenomenon in which some grains grow rapidly while other grains remain smaller in size. It is possible that the material generates local stress, causing some grains to grow rapidly. It is also possible that the chemical composition is uneven or there are impurities similar to copper, resulting in different grain growth rates in different areas.

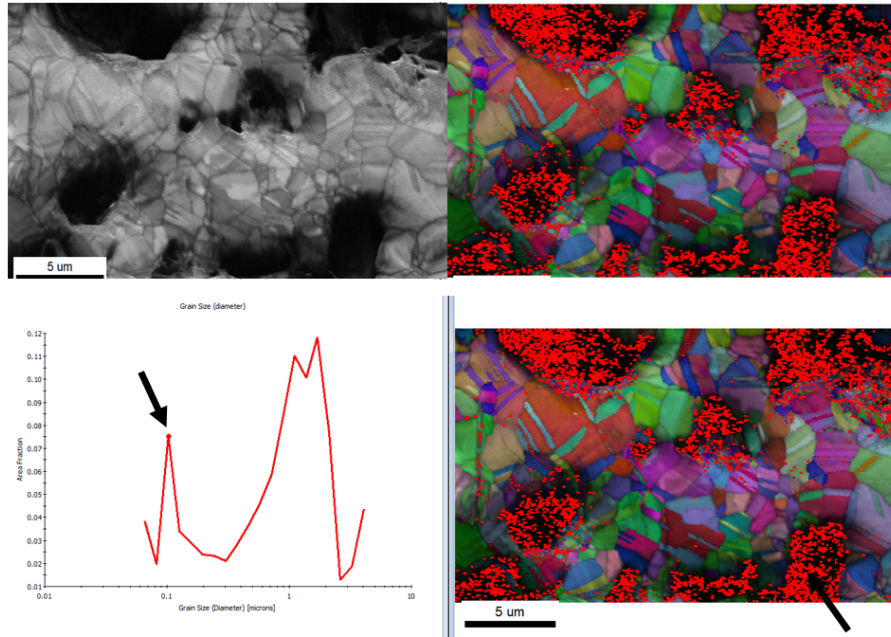


Figure 3.25: Comparison of grain size with IPF+TOP figure

However, as shown in **Figure 3.25**, the reason why many smaller grain sizes appear in the first peak is that many small grain sizes appear near the hole. It may be difficult to identify the grain in this place because it is a hole, or it may be because the surface is concave due to the hole, so this area cannot be identified. So, the grain size distribution of the aging test in Nitrogen only has one peak and still aligns with normal grain growth.

Grain Growth Model

Grain growth usually follows the following empirical formula:

$$D^n - D_0^n = K \cdot t$$

which

- D is the average grain size(Area) at time t ,
- D_0 is the initial grain size(Area),
- n is the grain growth exponent,
- K is a temperature-dependent constant,
- t is the aging time.

By fitting the grain growth data of the L1 and L3 groups, the following grain growth index n is obtained:

- The grain growth index $n = 1.53$ (approximately) of the Air group indicates that the grain growth process is close to linear.
- The grain growth index $n = 2.13$ of the Nitrogen group indicates that the grain growth rate of the L3 group is relatively slow, which may be affected the atmosphere.

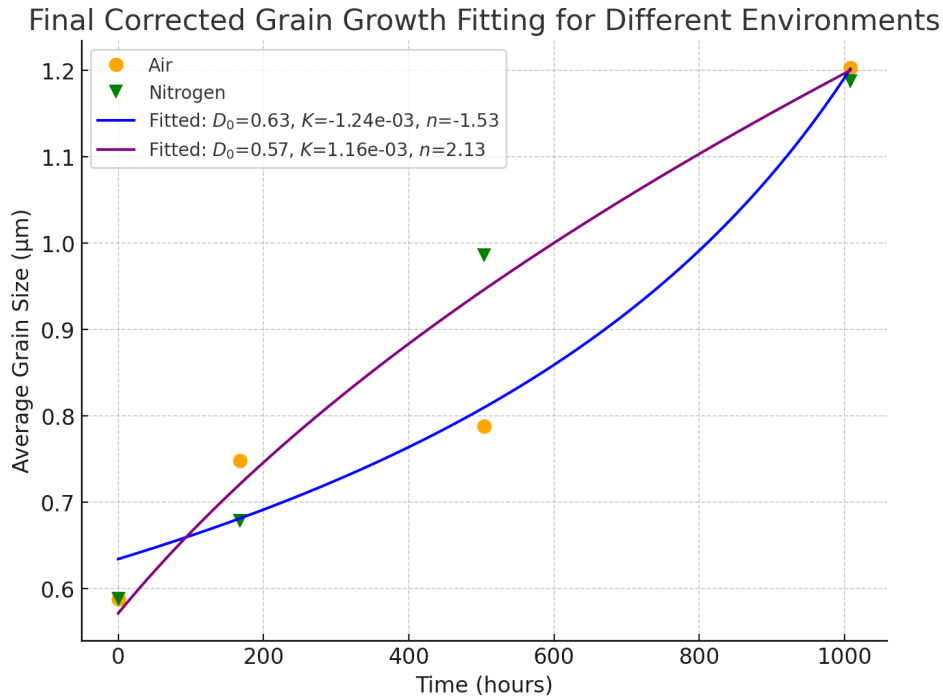


Figure 3.26: Grain growth fitting curves of L1 and L3 groups

The figure above shows the grain growth curves of the Air and Nitrogen groups. It can be seen that the grain growth index of the nitrogen group is larger, while the grain growth index of the oxygen group tends to 0, which indicates that the growth trend of the data shows an extremely slow change in the air environment, resulting in the model being unable to identify obvious growth dynamics characteristics.

Dislocation Density and Plastic Deformation Analysis Using KAM

Kernel Average Misorientation (KAM) is used to analyze the microstructure of materials, especially the deformation and defect distribution within the grains. It reflects the degree of plastic deformation by measuring the orientation change of the local area within the grain. A higher KAM value usually indicates a higher dislocation density. The KAM value reflects the dislocation density and degree of deformation inside the material. The colors from blue to red represent the increase of KAM values. The bluer the color, the smaller the change in crystal orientation. The redder the color, the larger the orientation difference, which means that a larger plastic deformation has occurred inside the material.

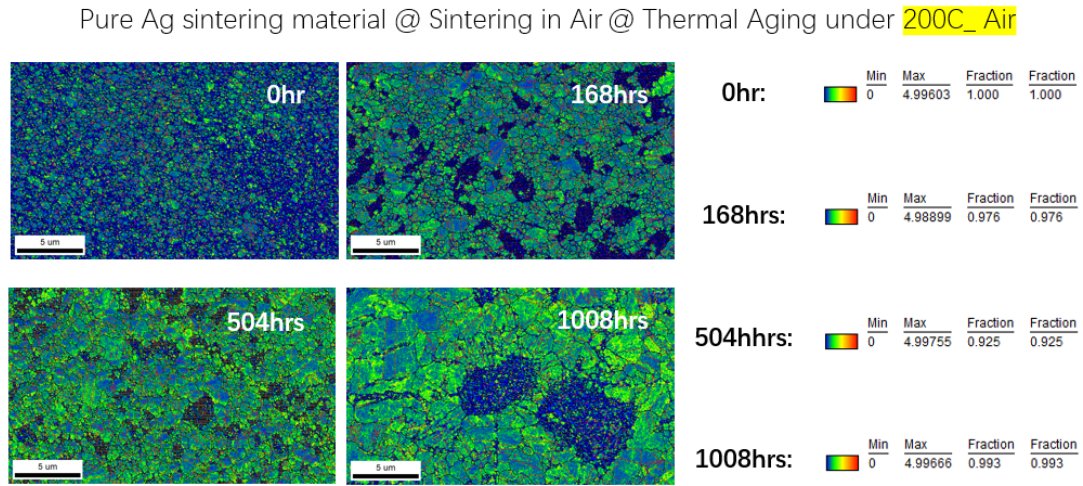


Figure 3.27: Kernel Average Misorientation figure of thermal aging of pure silver sintered material at 200°C in air environment

This picture shows the KAM diagram of the material at 200°C (L1E) in the air environment. At 0 hours, the interior of the material mainly appears blue and green, and the KAM value is small, indicating that the dislocation density is low and the material structure is relatively stable. After 168 hours, more green and yellow areas gradually appeared in the material, indicating that the plastic deformation in local areas began to intensify. By 504 hours, a significant increase in green areas and the appearance of localized yellow areas can be observed. Finally, at 1008 hours, the yellow area is more obvious, especially in the large grain area, indicating that the internal stress of the material is concentrated at this time.

As the aging time increases, the KAM value of the material gradually increases, indicating that the local orientation difference within the material increases, the dislocation density increases, and the plastic deformation intensifies.

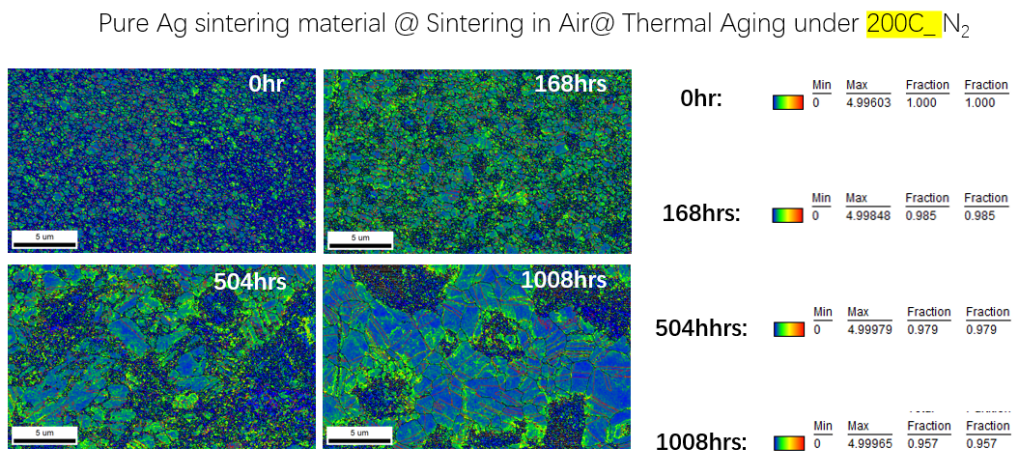


Figure 3.28: Kernel Average Misorientation figure of thermal aging of pure silver sintered material at 200°C in nitrogen environment

This picture shows the KAM picture of the material at 200°C (L3E) in a nitrogen environ-

ment. At 0 hours, the material shows a low KAM value, indicating that the dislocation density is low and the grains are relatively stable. At 168 hours, more green and yellow colors appear in some areas, and the dislocation density within the material increases. By 504 hours, the green area increased significantly, indicating an increase in dislocation density. Finally, after 1008 hours, the yellow area in the material increased and the KAM value increased significantly, indicating higher dislocation density and increased plastic deformation.

Compared with the air environment, thermal aging in a nitrogen environment causes the material's plastic deformation rate to be relatively slow and the accumulation of dislocations to be less. This may be due to the inert nature of nitrogen that inhibits the oxidation process, thus slowing down the development of deformation. This suggests that the oxidative effects in air accelerate dislocation accumulation and plastic deformation, while the inert environment of nitrogen retards these evolution processes.

4

Modelling and Simulation

4.1. Modelling of Microstructural Evolution

After completing all the experiments, we came to some conclusions. For example, in an air environment, oxidation will make the pores larger, and uneven grain growth will increase the possibility of abnormal grain growth, resulting in changes in the material microstructure, showing more dislocations, and thus significantly reducing the mechanical properties of the material; while a nitrogen environment will inhibit the degradation of the sintered silver material, maintain a relatively stable grain structure, the material plastic deformation rate is slow, and the dislocation density increase is relatively small. In a formic acid vapor environment, the degradation of the sintered silver material will be further inhibited. These phenomena can all illustrate that the ambient atmosphere has a significant effect on the evolution of the material microstructure, especially during long-term processing at high temperatures. On a time scale, as the aging time increases, the mechanical properties of the material continue to deteriorate, and the pores in the sintered silver layer continue to grow.

But using simulations to predict the long-term microstructural evolution under different temperature and atmosphere conditions is needed. Simulation studies will help with more fully understand the life and reliability of the material in a real environment. It can also verify experimental results and help understand microscopic mechanisms, such as the movement of dislocations, to optimize the design. At the same time, the quantitative parameters obtained in the experiment can better help establish simulation models for mutual verification. Therefore, simulation is a powerful supplement and extension of experimental research.

4.1.1. Kinetic Monte Carlo simulation & Potts model

KMC is a method for simulating the time evolution of a system. KMC simulates the occurrence of changes by random sampling and determines the state changes of the system by probabilistic rules.

The Potts model is commonly used to simulate grain growth and recrystallization. Also, Potts model is a statistical mechanical model that utilizes Monte Carlo methods to evolve an ensemble of discrete particles, or sites, defined on a lattice. This ensemble of sites represents the material microstructure. Each lattice site i assumes a spin, q_i , that represents a given feature of the microstructure, such as membership in a grain or phase. The total energy of the system

is given by summing the bulk energy, E_v , at each site and the interfacial energy, J , between the site and its neighboring lattice sites j . This total energy is given as:

$$E_{Potts} = \sum_{i=1}^N \sum_{j=1}^n J(q_i, q_j) \quad (4.1)$$

where N represents the total number of sites, and the interfacial energy for each site is determined by summing the function J , defined as:

$$J = \begin{cases} 1, & \text{if } q_i \neq q_j \\ 0, & \text{if } q_i = q_j \end{cases} \quad (4.2)$$

The Potts Model has been successfully employed to study grain growth (including the effects of grain boundary migration and anisotropy, and abnormal grain growth), recrystallization, Zener Pinning, growth coalescence, and sintering. The very stable framework of the Potts model provides the ability to study any number of microstructure evolution characteristics in a statistically representative manner.

4.1.2. KMC-based hybrid Q-state potts & phase field model (QPPF)

In the Potts-Phase Field model, the total energy of the system depends not only on the interaction between the grid site but also on the composition of the material and the coupling energy between the state and the phase composition. The total energy of system can be written as

$$E_{Hybrid} = \sum_{i=1}^N (E_v(q_i, C_i) + \sum_{j=1}^n J(q_i, q_j) + \kappa_C (\nabla C_i)^2) \quad (4.3)$$

The phase field method is widely used to simulate various processes at the microstructural level. The practical application range of this method ranges from solidification and solid-state phase transformation to sintering processes. Microstructural changes in the phase field method are handled by considering the time evolution of multiple phase field variables. These variables represent the structural or chemical order at any location within the material. This method can be used to characterize and simulate the movement of diffusion interfaces formed between different phases or domains[16].

The hybrid model is based on the Q-state Potts and phase field models, simulating phase changes in materials and handling evolutions related to material composition. With this combination, the QPPF model can more accurately describe the microstructural evolution in multiphase materials.

The Q-state Potts model mentioned above is most importantly simulated by energy functions. At the same time, the phase field model simulates the composition changes of the material. The phase field model describes the evolution of the material composition C , and uses the volumetric free energy function `volumetric_free_energy` to calculate the free energy of each grid point. The free energy function is determined by the composition C and the phase q , and the formula is:

$$E_v = k ((C - C_1)^2 + (C_2 - C)^2) + \alpha ((C - C_3)^2 q_A + (C_4 - C)^2 q_B) \quad (4.4)$$

Where C_1, C_2, C_3, C_4 are parameters that control the minimum free energy, α is the coupling coefficient, and q_A and q_B are used to identify the states of different phases[16].

A core of the QPPF model is the evolution of coupled phases and compositions. In each Monte Carlo step, the phase state of the grid is updated by the Potts model, and the composition field evolves by the phase field equation. The time evolution equation of the composition is:

$$\frac{\partial C}{\partial t} = M_c \left\{ \nabla^2 \left(\frac{\partial E_v}{\partial C} \right) - \kappa \nabla^4 C \right\} \quad (4.5)$$

Where M_c is the mobility, κ is the gradient interface energy constant. The larger the κ , the sharper the interface Gradient Plasticity Theory will be.. Through this synchronous evolution, the QPPF model can accurately capture the complex dynamic changes of materials between different phases and compositions[16].

Overall, the KMC-based hybrid Q-state Potts and phase field model (QPPF) can both simulate the phase change of materials and observe the evolution of compositions, combining discrete phase change and continuous composition change.

4.2. Simulation Results and Analysis

Pure Ag sintering material @ Sintering in Air @ Start from 0h

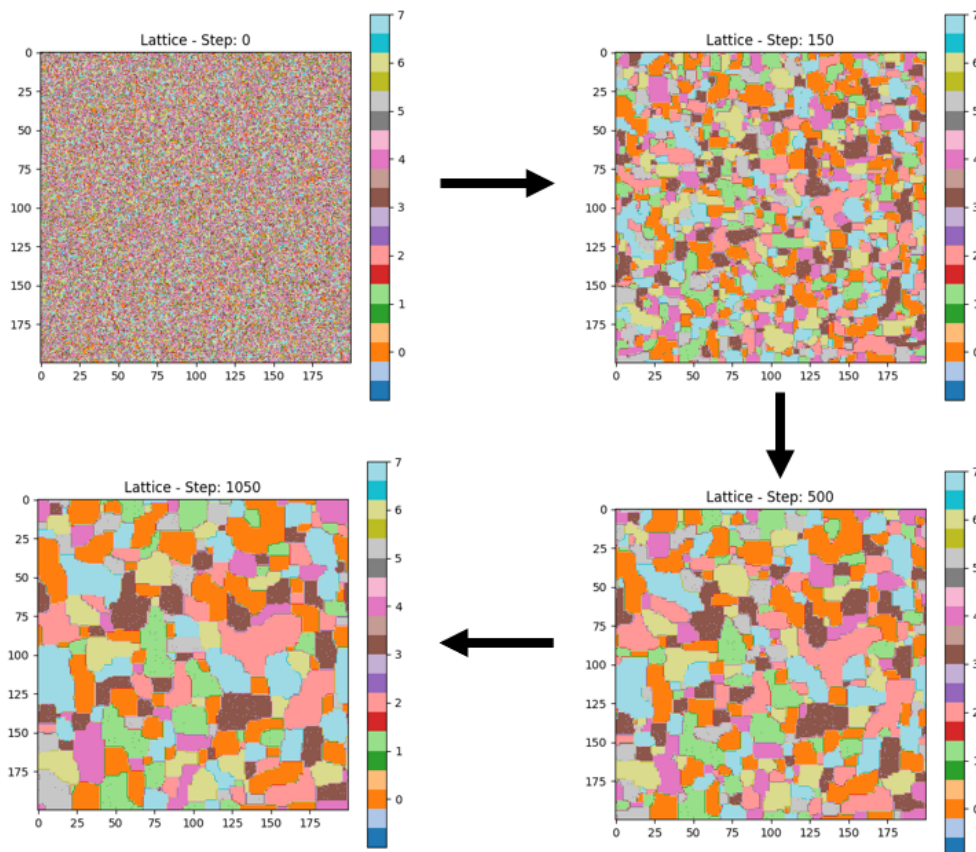


Figure 4.1: Simulation of the microstructure evolution of pure silver sintered material during sintering in air (starting from 0 hours)

Figure4.1 shows the evolution of the microstructure of the material during the sintering process in air (L1). The changes in the material's microstructure at different time steps and the entire process of grain growth evolution can be observed.

In the initial state, the microstructure of the material is characterized by very fine and dispersed grains. Different colors in the figure represent grains of different orientations. These grains are small in size, closely distributed, and the overall structure is relatively uniform. As the sintering process progresses, when Step 150 (corresponding to 168h) is reached, the grains begin to grow significantly and rearrange. Compared with the initial state, some larger grains begin to appear at this stage, but most of the grains are still small. When Step 500 (corresponding to 504h) is reached, the grain growth trend is more obvious, and the smaller grains are gradually swallowed by the larger grains, resulting in a further reduction in the number of grain boundaries. By Step 1050 (corresponding to 1008h), the grain growth gradually stabilizes, and large grains dominate the organization. The reduction of grain boundaries makes the internal structure of the material tend to be consistent. In the final state, the organization of the material has reached a relatively stable state, and the changes are no longer as drastic as before. Large grains occupy almost the entire image, and the proportion of fine grains is significantly reduced and almost disappears. A relatively uniform grain distribution is formed, but there are still some irregular shapes and differences between grains.

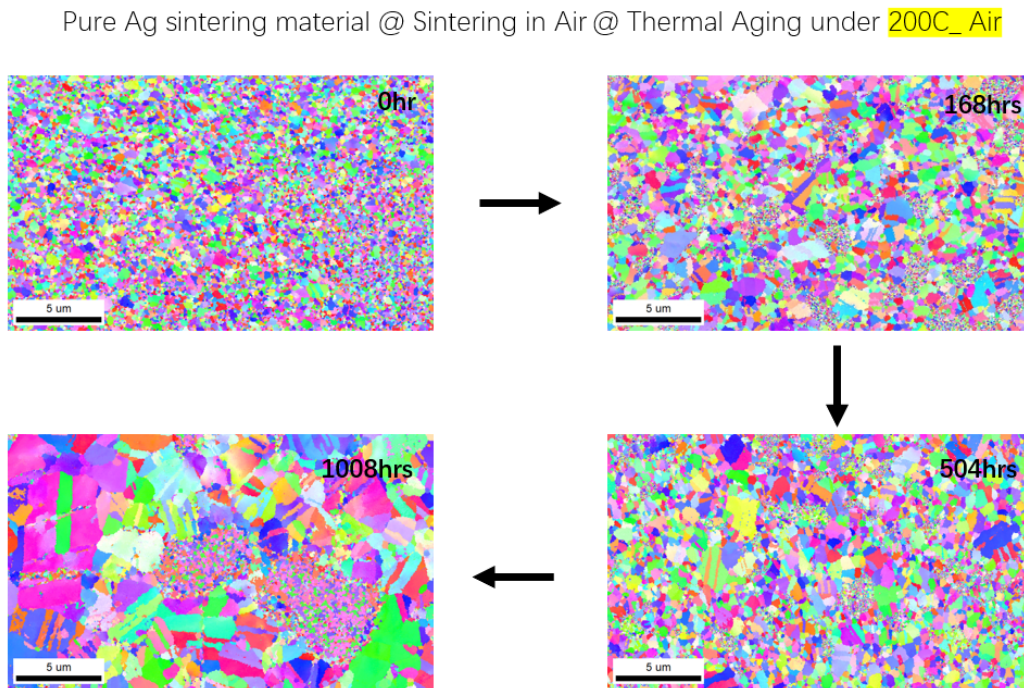


Figure 4.2: Microstructure evolution of pure silver sintered material during sintering in air (0h, 168h, 504h, 1008h)

Figure4.2 shows the IPF with microstructural evolution of the material during thermal aging at 200 °C in air (0h, 168h, 504h, 1008h). With the increase of aging time, the grains gradually change from fine to larger structures, and the number of grain boundaries decreases. By comparison, it is found that this trend is consistent with the different step length stages (Step 0 to 1050) in the simulation results, both showing the process of grain growth and fusion.

However, in actual situations, more changes in twins and voids will be observed, including the situation where there are still some small grains around large grains, especially in the later stages of aging. These results together show the dynamic evolution of pure silver materials during sintering and thermal aging in air.

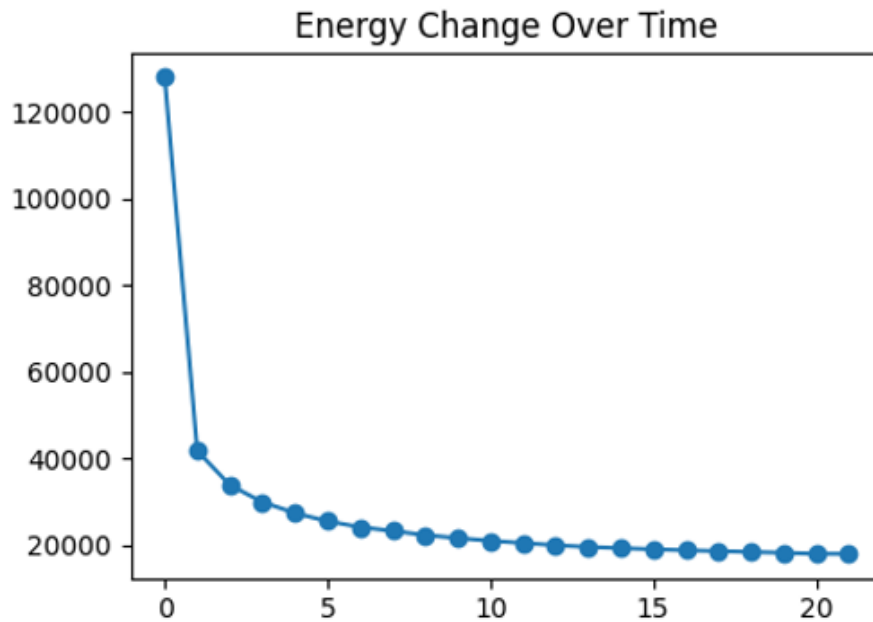


Figure 4.3: Energy change over time during system stabilization

Figure 4.3 shows the energy trend over time. As can be seen, the energy drops very quickly in the initial time steps, then slows down and levels off. This trend usually indicates that the system adjusts quickly from the initial state and then gradually settles to a stable state.

Pure Ag sintering material @ Sintering in Air @ Start from 0h

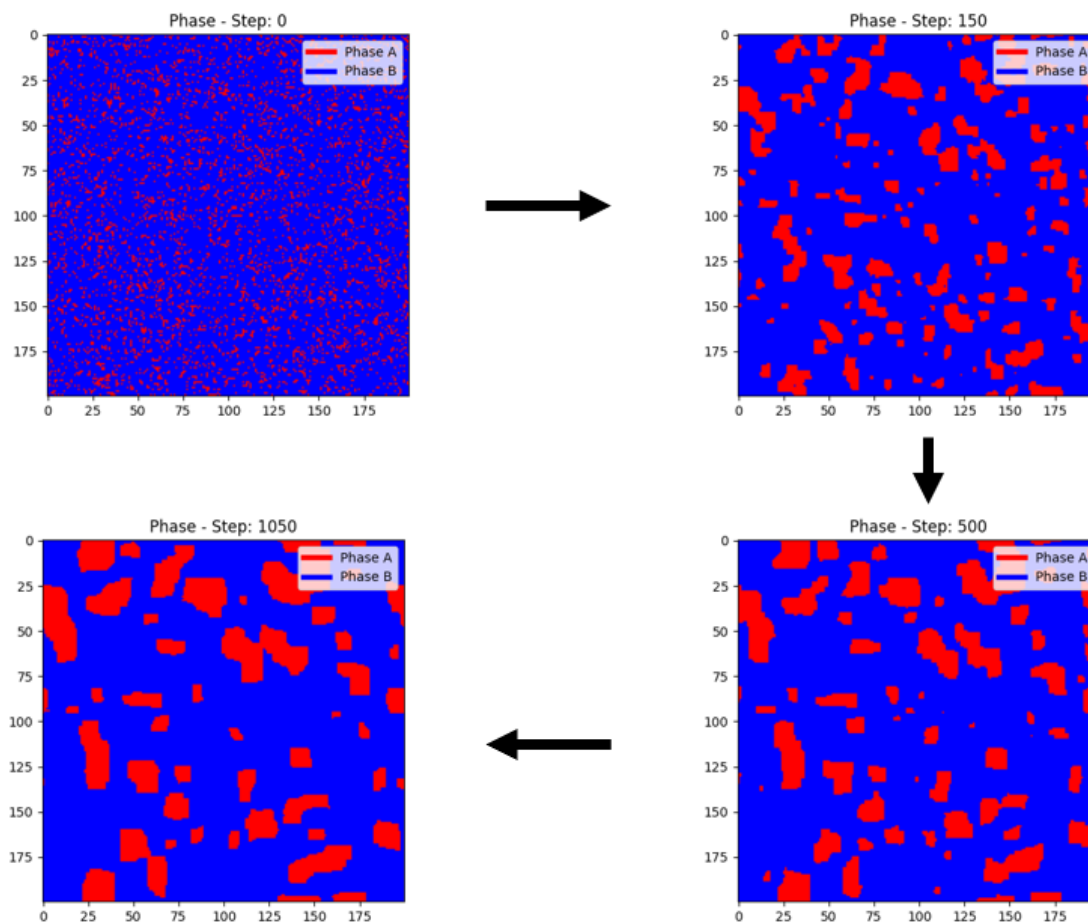


Figure 4.4: Phase evolution during aging process under air environment

The above figure corresponds to the different microstructural evolutions of the material during the aging process.

Phase B(Blue) may represent a relatively stable silver-based phase during the aging process, which is less affected by aging. Phase B has many states, and different states represent different grain orientations. Phase A(Red) may correspond to the pore structure of silver during the aging process. These pores are more numerous and widely distributed at the beginning of aging. As the aging time increases, these pores may redistribute and merge.

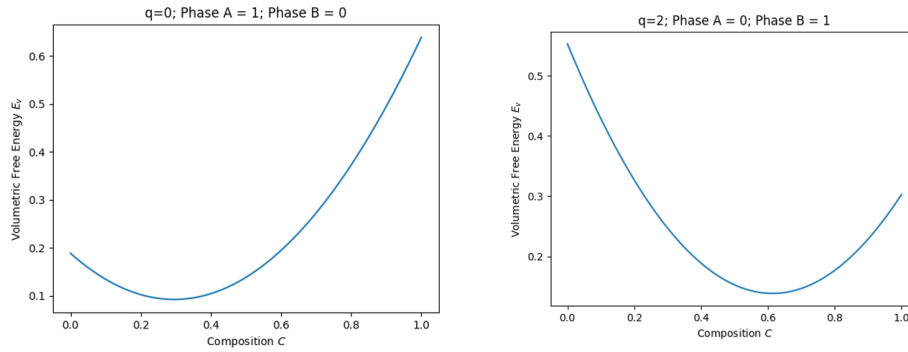


Figure 4.5: Volumetric free energy variation with composition for different phases

Figure 4.5 shows the relationship between composition C and volume free energy (E_v). In the left figure, it is the state of $q=0$, and Phase A is defined as the pore and Phase B is the silver state. The figure presents a typical parabolic shape, indicating that the free energy reaches a minimum value at around 0.3. This minimum point means that at this composition ratio, the system is in the most stable state. The right figure shows the state of silver at $q=2$, and Phase A is defined as the pore and Phase B is defined as the silver state. At around 0.6, the free energy reaches a minimum value and the system is most stable.

4.3. Limitations of the Model

Although this model performs well in simulating the microstructural evolution of multiphase materials, it still has some limitations. The model improves the efficiency of handling large-scale microstructures, but the computational efficiency needs to be further optimized in multiphase systems. At the same time, in order to be applied to real materials, the thermodynamic and kinetic parameters must be further matched.

5

Conclusion

In this study, the sintering and thermal aging processes of pure silver under different atmosphere conditions were analyzed in detail, revealing the evolution of the material's microstructure and its impact on mechanical properties. Through simulation and experimental data, we can clearly see that over time, the silver grains gradually grow, the number of grain boundaries decreases, and the pores inside the material decrease, showing a transition from a fine grain structure to a coarse grain structure.

In an air environment, oxidation significantly accelerates grain growth and pore expansion, making the microstructure of the material change more drastically. High-temperature oxidation leads to the weakening of grain boundaries and the increase of pores, forming an irregular grain structure, which affects the overall mechanical strength and durability of the material. During the long-term aging process, the material in the air environment shows a faster performance degradation, especially after 1008 hours, the crack extension and pore growth of the material are more obvious, and the mechanical strength is greatly reduced.

Relatively speaking, the protective effect of the nitrogen environment on the material is more significant. As an inert gas, nitrogen can effectively inhibit the oxidation process of silver, thereby slowing down the abnormal growth of grains and the expansion of pores. In a nitrogen environment, the microstructure of the material evolves more slowly, the pore growth rate is lower, the overall structure is more uniform, and it shows better mechanical properties and stability. Nevertheless, even in a nitrogen environment, the internal structure of the material still inevitably ages over time, including pore expansion and weakened connections between grains.

The comparison between the experimental and simulation results further verifies these conclusions. The simulation shows the trend of grain growth and structural coarsening during sintering, which is highly consistent with the structural changes revealed by the microscopic images at different time periods in the experiment. The changes in grain morphology, pore distribution, and overall degradation rate of the material in the air environment are consistent with the rapid growth stage in the simulation results, while the structural changes in the nitrogen environment reflect the relatively stable grain evolution process in the simulation results.

In summary, this study shows that the sintering and aging processes of pure silver materials show significant differences in different atmospheres. By heat treating in a nitrogen environment, the service life of the material can be more effectively extended and relatively stable

mechanical properties can be maintained, while the rapid oxidation and structural degradation in the air environment require special attention and improvement.

Bibliography

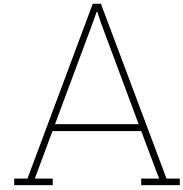
- [1] <https://www.panacol.com/adhesive-applications/smart-card/die-attach-electrically-conductive-adhesives>.
- [2] <https://www.emergenresearch.com/cn/industry-report/big-data-analytics-in-manufacturing-market>.
- [3] <https://chinese.alibaba.com/product-detail/REG101NA-A3K-Original-Ic-Chip-Single-1601135123001.html>.
- [4] Ousama M Abdelhadi and Leila Ladani. “IMC growth of Sn-3.5 Ag/Cu system: Combined chemical reaction and diffusion mechanisms”. In: *Journal of Alloys and Compounds* 537 (2012), pp. 87–99.
- [5] Hani Alarifi et al. “Silver nanoparticle paste for low-temperature bonding of copper”. In: *Journal of Electronic Materials* 40 (2011), pp. 1394–1402.
- [6] John Bai et al. “Low-Temperature Sintered Nanoscale Silver as a Novel Semiconductor Device-Metallized Substrate Interconnect Material”. In: *Components and Packaging Technologies, IEEE Transactions on* 29 (Oct. 2006), pp. 589 –593. DOI: 10 . 1109 / TCAPT . 2005 . 853167.
- [7] B Chalmers, R King, and R Shuttleworth. “The thermal etching of silver”. In: *Proceedings of the Royal Society of London. Series A. Mathematical and Physical Sciences* 193.1035 (1948), pp. 465–483.
- [8] Chuantong Chen et al. “Effect of oxygen on Ag sintering technology with low temperature pressureless”. In: *2018 19th International Conference on Electronic Packaging Technology (ICEPT)*. IEEE. 2018, pp. 15–18.
- [9] Chuantong Chen et al. “Effect of oxygen on microstructural coarsening behaviors and mechanical properties of Ag sinter paste during high-temperature storage from macro to micro”. In: *Journal of Alloys and Compounds* 834 (2020), p. 155173.
- [10] Ui-Min Choi, Frede Blaabjerg, and Kyo-Beum Lee. “Study and handling methods of power IGBT module failures in power electronic converter systems”. In: *IEEE Transactions on Power Electronics* 30.5 (2014), pp. 2517–2533.
- [11] ST Chua, KS Siow, and A Jalar. “Effect of sintering atmosphere on the shear properties of pressureless sintered silver joint”. In: *36th International Electronics Manufacturing Technology Conference*. IEEE. 2014, pp. 1–6.
- [12] M Ferrante and RD Doherty. “Influence of interfacial properties on the kinetics of precipitation and precipitate coarsening in aluminium-silver alloys”. In: *Acta Metallurgica* 27.10 (1979), pp. 1603–1614.
- [13] A Frøseth, H Van Swygenhoven, and PM Derlet. “The influence of twins on the mechanical properties of nc-Al”. In: *Acta Materialia* 52.8 (2004), pp. 2259–2268.

- [14] Alarifi HA et al. “Molecular dynamics simulation of sintering and surface premelting of silver nanoparticles”. In: *Materials Transactions* 54.6 (2013), pp. 884–889.
- [15] Akio Hirose et al. “A novel metal-to-metal bonding process through in-situ formation of Ag nanoparticles using Ag₂O microparticles”. In: *Journal of Physics: Conference Series*. Vol. 165. 1. IOP Publishing. 2009, p. 012074.
- [16] Eric R Homer, Veena Tikare, and Elizabeth A Holm. “Hybrid Potts-phase field model for coupled microstructural–compositional evolution”. In: *Computational materials science* 69 (2013), pp. 414–423.
- [17] Dong Hu et al. “High temperature viscoplastic deformation behavior of sintered nanocopper paste used in power electronics packaging: Insights from constitutive and multi-scale modelling”. In: *Journal of Materials Research and Technology* 26 (2023), pp. 3183–3200. ISSN: 2238-7854. DOI: <https://doi.org/10.1016/j.jmrt.2023.08.086>. URL: <https://www.sciencedirect.com/science/article/pii/S2238785423018987>.
- [18] Dong Hu et al. “Thermal kinetic and mechanical behaviors of pressure-assisted Cu nanoparticles sintering: A molecular dynamics study”. In: *Results in Physics* 19 (2020), p. 103486.
- [19] Xiao Hu et al. “Sintering Process Simulation of Ag Nanoparticles by Phase Field Method”. In: *2024 25th International Conference on Thermal, Mechanical and Multi-Physics Simulation and Experiments in Microelectronics and Microsystems (EuroSimE)*. 2024, pp. 1–6. DOI: 10.1109/EuroSimE60745.2024.10491517.
- [20] Seonhee Jang and Muhibbur Rahman. “Effect of sintering atmospheres on printed silver nanoparticle patterns for flexible electronics application”. In: *Applied Physics A* 127 (2021), pp. 1–14.
- [21] Jinting Jiu et al. “A new micro-silver paste for high power semiconductor devices”. In: *2016 China Semiconductor Technology International Conference (CSTIC)*. IEEE. 2016, pp. 1–3.
- [22] John G Kassakian and Thomas M Jahns. “Evolving and emerging applications of power electronics in systems”. In: *IEEE Journal of Emerging and Selected Topics in Power Electronics* 1.2 (2013), pp. 47–58.
- [23] Tomi Laurila, Vesa Vuorinen, and JK Kivilahti. “Interfacial reactions between lead-free solders and common base materials”. In: *Materials Science and Engineering: R: Reports* 49.1-2 (2005), pp. 1–60.
- [24] Wen-Hua Li et al. “Low-temperature Cu-to-Cu bonding using silver nanoparticles stabilised by saturated dodecanoic acid”. In: *Materials Science and Engineering: A* 613 (2014), pp. 372–378.
- [25] Chun-An Lu et al. “Effects of metallo-organic decomposition agents on thermal decomposition and electrical conductivity of low-temperature-curing silver paste”. In: *Japanese journal of applied physics* 45.9R (2006), p. 6987.
- [26] Qing Ma and David R Clarke. “Size dependent hardness of silver single crystals”. In: *Journal of Materials research* 10.4 (1995), pp. 853–863.

- [27] X Milhet et al. “Evolution of the nanoporous microstructure of sintered Ag at high temperature using in-situ X-ray nanotomography”. In: *Acta Materialia* 156 (2018), pp. 310–317.
- [28] Jose Millan et al. “A survey of wide bandgap power semiconductor devices”. In: *IEEE transactions on Power Electronics* 29.5 (2013), pp. 2155–2163.
- [29] John A Mitchell et al. “Parallel simulation via SPPARKS of on-lattice kinetic and Metropolis Monte Carlo models for materials processing”. In: *Modelling and Simulation in Materials Science and Engineering* 31.5 (2023), p. 055001.
- [30] Fengwen Mu et al. “Mechanism of low temperature sintering-bonding through in-situ formation of silver nanoparticles using silver oxide microparticles”. In: *Materials Transactions* 54.6 (2013), pp. 872–878.
- [31] Habib A Mustain, William D Brown, and Simon S Ang. “Transient liquid phase die attach for high-temperature silicon carbide power devices”. In: *IEEE transactions on components and packaging technologies* 33.3 (2010), pp. 563–570.
- [32] Luis A Navarro et al. “Thermomechanical assessment of die-attach materials for wide bandgap semiconductor devices and harsh environment applications”. In: *IEEE transactions on Power Electronics* 29.5 (2013), pp. 2261–2271.
- [33] Chulmin Oh et al. “Effect of oxygen on pressureless silver sintering in a nitrogen atmosphere”. In: *Journal of Materials Science: Materials in Electronics* 31 (2020), pp. 488–494.
- [34] Keunju Park, Dongseok Seo, and Jongkook Lee. “Conductivity of silver paste prepared from nanoparticles”. In: *Colloids and Surfaces A: Physicochemical and Engineering Aspects* 313-314 (2008). Nanoscience and Nanotechnology, pp. 351–354. ISSN: 0927-7757. DOI: <https://doi.org/10.1016/j.colsurfa.2007.04.147>. URL: <https://www.sciencedirect.com/science/article/pii/S0927775707005304>.
- [35] Sunghyun Park, Dongseok Seo, and Jongkook Lee. “Preparation of Pb-free silver paste containing nanoparticles”. In: *Colloids and Surfaces A: Physicochemical and Engineering Aspects* 313 (2008), pp. 197–201.
- [36] Peng Peng et al. “Joining of silver nanomaterials at low temperatures: processes, properties, and applications”. In: *ACS applied materials & interfaces* 7.23 (2015), pp. 12597–12618.
- [37] SM Sajjad Hossain Rafin et al. “Power Electronics Revolutionized: A Comprehensive Analysis of Emerging Wide and Ultrawide Bandgap Devices”. In: *Micromachines* 14.11 (2023), p. 2045.
- [38] Marco Schaal, Markus Klingler, and Bernhard Wunderle. “Silver sintering in power electronics: the state of the art in material characterization and reliability testing”. In: *2018 7th Electronic system-integration technology conference (ESTC)*. IEEE. 2018, pp. 1–18.
- [39] Marco Schaal, Markus Klingler, and Bernhard Wunderle. “Silver sintering in power electronics: the state of the art in material characterization and reliability testing”. In: *2018 7th Electronic system-integration technology conference (ESTC)*. IEEE. 2018, pp. 1–18.

- [40] Jagpreet Singh, Gurjas Kaur, and Mohit Rawat. “A brief review on synthesis and characterization of copper oxide nanoparticles and its applications”. In: *J. Bioelectron. Nanotechnol* 1.9 (2016).
- [41] K. S. Siow and Y. T. Lin. “Identifying the Development State of Sintered Silver (Ag) as a Bonding Material in the Microelectronic Packaging Via a Patent Landscape Study”. In: *Journal of Electronic Packaging* 138.020804 (Apr. 2016). ISSN: 1043-7398. DOI: 10.1115/1.4033069. URL: <https://doi.org/10.1115/1.4033069> (visited on 01/27/2021).
- [42] Kim S Siow. “Are sintered silver joints ready for use as interconnect material in microelectronic packaging?” In: *Journal of electronic materials* 43 (2014), pp. 947–961.
- [43] Kim S Siow. “Die-attach materials for high temperature applications in microelectronics packaging”. In: *Materials, Processes, Equipment, and Reliability*. Springer, 2019.
- [44] KS Siow and YT Lin. “Identifying the development state of sintered silver (Ag) as a bonding material in the microelectronic packaging via a patent landscape study”. In: *Journal of Electronic Packaging* 138.2 (2016), p. 020804.
- [45] KS Siow and YT Lin. “Identifying the development state of sintered silver (Ag) as a bonding material in the microelectronic packaging via a patent landscape study”. In: *Journal of Electronic Packaging* 138.2 (2016), p. 020804.
- [46] KS Siow et al. “Influence of sintering environment on silver sintered on copper substrate”. In: *Journal of Materials Science: Materials in Electronics* 30 (2019), pp. 6212–6223.
- [47] Chih-Han Tseng et al. “Kinetic study of grain growth in highly (111)-preferred nanotwinned copper films”. In: *Materials Characterization* 168 (2020), p. 110545. ISSN: 1044-5803. DOI: <https://doi.org/10.1016/j.matchar.2020.110545>. URL: <https://www.sciencedirect.com/science/article/pii/S1044580320320167>.
- [48] MV Uvarajan et al. “Temperature cycling aging studies of Zn-based solders for high-temperature applications”. In: *2015 IEEE 17th Electronics Packaging and Technology Conference (EPTC)*. IEEE, 2015, pp. 1–5.
- [49] Leong Ching Wai et al. “Study on silver sintered die attach material with different metal surfaces for high temperature and high pressure (300°C/30kpsi) applications”. In: *2013 IEEE 15th Electronics Packaging Technology Conference (EPTC 2013)*. 2013, pp. 335–340. DOI: 10.1109/EPTC.2013.6745738.
- [50] Seunghwa Yang, Wonbae Kim, and Maenghyo Cho. “Molecular dynamics study on the coalescence kinetics and mechanical behavior of nanoporous structure formed by thermal sintering of Cu nanoparticles”. In: *International Journal of Engineering Science* 123 (2018), pp. 1–19.
- [51] Min Yi et al. “Modeling and simulation of sintering process across scales”. In: *Archives of Computational Methods in Engineering* 30.5 (2023), pp. 3325–3358.
- [52] Min Yi et al. “Modeling and simulation of sintering process across scales”. In: *Archives of Computational Methods in Engineering* 30.5 (2023), pp. 3325–3358.

- [53] Fang Yu, R. Wayne Johnson, and Michael C. Hamilton. “Pressureless Sintering of Microscale Silver Paste for 300 °C Applications”. In: *IEEE Transactions on Components, Packaging and Manufacturing Technology* 5.9 (2015), pp. 1258–1264. DOI: 10.1109/TCPMT.2015.2455811.
- [54] Guang Zeng, Stuart McDonald, and Kazuhiro Nogita. “Development of high-temperature solders”. In: *Microelectronics Reliability* 52.7 (2012), pp. 1306–1322.
- [55] HongWen Zhang and Ning-Cheng Lee. “A novel high melting lead-free mixed solder paste system”. In: *2011 IEEE 13th Electronics Packaging Technology Conference*. IEEE. 2011, pp. 567–572.
- [56] Zheng Zhang et al. “Ag-Ag direct bonding via a pressureless, low-temperature, and atmospheric stress migration bonding method for 3D integration packaging”. In: *2022 IEEE 72nd Electronic Components and Technology Conference (ECTC)*. IEEE. 2022, pp. 1409–1412.



Pseudocode

The following pseudocode describes the main function workflow of Q-state Potts-Phase Field (QPPF), a simulation tool designed by the Electronic Components, Technology and Materials research group at TU Delft. It provides a graphical user interface (GUI) for users to set simulation parameters such as lattice size, number of states, temperature, number of Monte Carlo steps, etc. The Taichi Language Python package compiles it to support high-efficiency parallel computation. This tool can simulate the co-evolution of grain and composition through the hybrid potts-phase field model. Users can choose to initialize the lattice with an image, add fixed points, and choose to load or unload a hybrid Potts-phase field model. The simulation results can be visualized as a lattice map, phase distribution map, composition map, and energy changes, and this tool provides supporting functions such as image saving and free energy calculation.

```
1   # Constructor initializes lattice, composition, and energy fields
2   Initialize with lattice size L and number of states Q
3       Create a 2D array for the lattice with shape (L, L)
4       Create a 2D array for the composition with shape (L, L)
5       Create vectors to store positions of pins
6       Initialize fields for energy calculations
7
8   # Initialize the lattice randomly with states between 0 and Q
9   Method initialize_lattice:
10      For each element in the lattice:
11          Assign a random integer value between 0 and Q
12
13  # Initialize the composition based on lattice values
14  Method initialize_composition:
15      For each element in the lattice:
16          If the lattice value represents phase A:
17              Assign a random composition between 0.0 and 0.5
18          If the lattice value represents phase B:
19              Assign a random composition between 0.5 and 1.0
20          Else:
21              Assign a random composition between 0.3 and 0.6
22
23  # Initialize the lattice using an image as input
24  Method initialize_lattice_from_image(image_path):
```

```
25     Load the image from file
26     Resize the image to fit the lattice size
27     Convert image pixel values to lattice states
28
29     # Add pins to fixed positions in the lattice
30     Method add_pins(num_pins):
31         Select random positions on the lattice
32         Store these positions in the pins vector
33
34     # Perform a Monte Carlo step using Glauber dynamics
35     Method glauber_step():
36         Repeat L*L times (one for each lattice point):
37             Randomly select a lattice point
38             If the point is pinned, skip
39             Generate a new random state different from the current state
40             Calculate the energy change from switching states
41             If the energy decreases or a probability condition is met,
42                 update the state
43
44     # Calculate the energy difference between the current and proposed
45     states
46     Method delta_energy():
47         Compute the interaction energy between neighbors for the old and
48         new states
49         If the hybrid model is used, also compute volumetric free energy
50
51     # Evolve the composition field based on a differential equation
52     Method evolve_composition():
53         For each lattice point:
54             Compute the Laplacian (second derivative) of the composition
55             field
56             Update the composition using a gradient flow approach
57
58     # Calculate the total energy of the system
59     Method compute_total_energy():
60         Initialize total energy to zero
61         For each lattice point:
62             Compute the interaction energy between neighbors
63             If hybrid model is used, add the free energy from the
64             composition
65         Return the total energy
```